Evaluation of Volatility and Thermal Stability in Monomeric and Dimeric Lanthanide(III) Complexes Containing Enaminolate Ligands

Navoda Jayakodiarachchi,[†] Paul G. Evans,[‡] Cassandra L. Ward,[†] and Charles H. Winter*[,†]

[†]Department of Chemistry, Wayne State University, Detroit, Michigan 48202

[‡]Department of Materials Science and Engineering, University of Wisconsin-Madison, Madison, Wisconsin 53706

ABSTRACT: Treatment of 3 equivalents of the potassium salts derived from the β-amino ketones 1-(dimethylamino)-3,3-dimethylbutan-2-one (L^1H), 3,3-dimethyl-1-(pyrrolidin-1-yl)butan-2-one (L^2H), or 3,3-dimethyl-1-(piperidin-1-yl)butan-2-one (L^3H) with anhydrous lanthanide(III) chlorides afforded the complexes $Ln(L^1)_3(L^1H)$ (Ln = Pr, Er, Y), $Ln(L^1)_3$ (Ln = Pr, Er, Lu, Y), $[Nd(L^1)_3]_2$, $[La(L^2)_3]_2$, and $Ln(L^3)_3$ (Ln = La, Pr, Nd, Er, Lu, Y) in 30 to 56% yields after crystallization from solvent or sublimation. X-ray crystal structures of $Ln(L^1)_3(L^1H)$, $Lu(L^1)_3$, $Er(L^3)_3$, and $Lu(L^3)_3$ revealed monomeric molecular structures, whereas $[Nd(L^1)_3]_2$ and $[La(L^2)_3]_2$ exist as dimers bridging through the oxygen atoms of two L^1 or L^2 ligands. The L^1, L^1H, L^2, and L^3 ligands exist mostly with bidentate coordination modes through the oxygen and nitrogen atoms. The new complexes sublime between 95 and 160 °C at 0.5 Torr. Thermogravimetric analysis traces of $Ln(L^1)_3(L^1H)$ (Ln = Pr, Er, Y) showed two step weight losses, with the first step entailing loss of L^1H. The other complexes demonstrated single step weight losses up to their decomposition temperatures. The complexes $Ln(L^3)_3$ (Ln = La, Pr, Nd, Er, Lu, Y) show the highest thermal stabilities among the new complexes, and are promising precursors for the growth of lanthanide-containing thin films by atomic layer deposition.

INTRODUCTION

Binary lanthanide(III) oxide thin films and ternary analogs containing other metal ions are of interest for applications as high dielectric constant (κ) materials in transistors and memory devices, since their κ values can be higher than currently used materials such as HfO_2.[1-9] Oxide thin films of the formula $LnAlO_3$ (Ln = La, Pr, Nd) grown on single crystal $SrTiO_3$ substrates have been studied in detail for their two-dimensional electron gas properties, where the electrical resistivities at the $LnAlO_3/SrTiO_3$ interfaces are very low.[10-16] For both high-κ dielectric applications and two-dimensional electron gas materials, the interfaces between the oxide materials and the substrates need to be atomically smooth for optimum performance.[10-17] Other applications of lanthanide-containing oxides include luminescent materials, optical materials, materials for quantum computing, superconductors, catalysis, and materials for advanced microelectronics.[18-25] While many methods can be used to deposit oxide films, atomic layer deposition (ALD) can afford films that are atomically smooth, in addition to providing Angstrom-level thickness control and perfect conformal coverage in high aspect ratio nanoscale features.[26,27] Increasingly, synthesis and crystallization methods are taking advantage of three-dimensional nanoscale features in which conformality and thickness uniformity of ALD are advantageous. The scope of applications of oxides created using ALD includes a range of optical and electronic devices incorporating nanoscale crystalline features.[28] The conformality and precision are possible because of the self-limited growth mechanism in ALD.

ALD requires chemical precursors that are volatile, thermally stable at the deposition temperatures, and highly reactive toward a second reagent.[26,27] Many different ligands have been employed to create volatile and thermally stable lanthanide precursors for film growth by ALD.[29] Ligands in previously reported precursors have included β-diketonate,[29-32] cyclopentadienyl and substituted cyclopentadienyl,[29,33-36] bis(trimethylsilyl)amide,[29] alkoxide,[29,37] and amidinates and guanidinates.[29,38-43] Additionally, volatile lanthanide complexes containing N,N-dimethylaminodiboranate ligands have been recently reported, but have not been tested in ALD growth.[44-46] Currently available lanthanide precursors have exhibited several problems in ALD growth, including the low reactivity of β-diketonate precursors towards water as a co-reactant, substrate oxidation when using ozone as a co-reactant, low thermal stability, and lack of true self-limited growth. As a result, there is ongoing need for volatile, thermally stable lanthanide precursors for ALD that address these issues.

In envisioning new structures that might lead to new volatile and thermally stable lanthanide complexes, we focused our attention on bidentate ligands that contain very strong bonds within the ligand backbones to promote high thermal stability. Enaminolate ligands L^1-L^3 (Scheme 1) are obtained upon deprotonation of β-amino ketones and contain a strong central C=C bond that should contribute high thermal stability to lanthanide complexes. The *tert*-butyl group is present to confer steric bulk, which should disfavor solvent coordination and may encourage monomeric complex formation. Moreover, there is only one acidic hydrogen atom site for enolate formation in ketones of

the formula $tBuC(=O)CH_2NR_2$, thereby eliminating the formation of isomeric enolates. Finally, the β-amino ketone $PhC(=O)CH_2NMe_2$ has a pKa value of 23.55,[47] which ensures that the the deprotonated enaminolates will react rapidly with water (pKa 14.00 or 15.7).[48] This situation should allow use of water as a co-reactant in ALD processes. There have been several reports of structurally characterized K, Ni, Zr, Zn, and P complexes containing enaminolate ligands that are similar to L^1-L^3.[49-52] No lanthanide complexes containing enaminolate complexes have been described to date. Herein, we report the synthesis, structure, volatility, and thermal stabilities of lanthanide complexes containing enaminolate ligands.

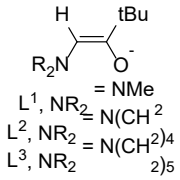

Scheme 1. Enaminolate ligands used in this study.

RESULTS AND DISCUSSION

Synthesis of New Complexes. The β-amino ketones L^1H-L^3H were prepared upon treatment of the bromomethyl ketone with secondary amines, as described in the Experimental Section. The potassium salts of L^1-L^3 were prepared by treatment of L^1H-L^3H with one equivalent of KH in THF. These freshly prepared solutions were treated directly with anhydrous $LnCl_3$ to afford complexes **1**-**15**, as outlined in equations 1-5 and in the experimental section.

Initial synthetic efforts explored treatment of $PrCl_3$, $ErCl_3$, and YCl_3 with three equivalents of KL^1 in THF. Workup, followed by crystallization from diethyl ether, led to slow crystallization of the L^1H adducts **1**-**3** in low, variable yields, apparently through partial hydrolysis and then formation of highly crystalline **1**-**3**. After obtaining X-ray crystal structures (vide infra), the syntheses of **1**-**3** were optimized by treatment of KL^1 (3 equiv) and L^1H (1 equiv) with $LnCl_3$ (Ln = Pr, Er, Y) to afford **1**-**3** in 30-36% yields after crystallization from diethyl ether (eq 1). The yields of **1**-**3** are low because of their high solubilities in diethyl ether. By contrast, sublimation of the crude reaction mixtures obtained upon treatment of KL^1 (3 equiv) with $LnCl_3$ (Ln = Pr, Er, Y) at 100 to 120 °C (0.5 Torr) afforded the homoleptic complexes **4**-**6** in 36-56% yields. Complexes **4**-**6** were also accessed upon sublimation of **1**-**3** in 42-52% yields, with loss of coordinated L^1H, as shown in equation 2. Sublimation of **1**-**3** was also accompanied by some decomposition to afford non-volatile residues, thus leading to the moderate yields. The remaining complexes **7**-**15** were obtained in 37-56% yields upon treatment of KL^1, KL^2, or KL^3 (3 equiv) with $LnCl_3$ (Ln = La, Pr, Nd, Er, Lu, Y) in THF (eqs 3-5), followed by sublimation at the temperatures described in the experimental procedures.

Complexes **1**-**15** were characterized by a combination of X-ray crystallography (**1**-**3**, **7**-**9**, **13**, **14**), ^1H nuclear magnetic resonance (NMR) spectroscopy (**3**, **6**, **8**-**10**, **14**, **15**), $^{13}C\{^1H\}$ NMR spectroscopy (**3**, **6**, **8**-**10**, **14**, **15**), infrared spectroscopy, melting points, and CHN microanalyses. ^1H NMR, $^{13}C\{^1H\}$ NMR, and infrared spectra are given in the Supporting Information (Figures S1-S31). The X-ray crystal structures are presented below and the line drawings in equations 1-5 represent the molecular structures that were observed for **1**-**3**, **7**-**9**, **13**, **14**. ^1H and $^{13}C\{^1H\}$ NMR spectra of the diamagnetic La, Lu, and Y complexes **3**, **6**, **8**-**10**, **14**, and **15** at ambient temperature in benzene-d_6 showed the expected resonances for L^1, L^1H, L^2, or L^3 ligands, as appropriate. The L^1-L^3 ligands in **3**, **6**, **8**-**10**, **14**, and **15** share common vinyl C-H and tBu moieties. The vinyl C-H resonances were observed as a sharp singlet in each spectrum between δ 4.55 and 4.96. The tBu groups appeared as a sharp singlet in each spectrum in the narrow range of δ 1.24 to 1.29. In the ^1H NMR spectrum of **3** at ambient temperature, separate resonances were observed for the L^1 and L^1H ligands, in a 3:1 ratio. The variable temperature ^1H NMR spectra of **3** are described below. The infrared spectra of **1**-**15** each show a medium to strong absorption between 1575 and 1618 cm^{-1} for the L^1, L^2, or L^3 C=C bonds and C-O single bond stretches between 1325 to 1337 cm^{-1}. For comparison, the C=O double bond stretches in L^1H-L^3H appear at 1717-1718 cm^{-1} and L^1H-L^3H do not show C=C or C-O single bond stretches. In addition to the L^1 C-O single bond stretches, the C=O double bond stretches for the coordinated L^1H ligands in **1**-**3** appear between 1678 and 1686 cm^{-1}. Complexes **1**-**10** and **12**-**15** gave H and N microanalysis values that were within ±0.4% of the calculated values. However, the C microanalysis values for **1**-**7**, **9**, **10**, and **12**-**15** were up to a few percent lower than the calculated values, despite multiple sample submissions and use of combustion enhancement. The lower C values in microanalyses might arise from refractory metal carbide formation. Several previous reports have reported similar low C microanalysis values in lanthanide complexes containing oxygen-based ligands.[53-57] Despite multiple submissions, **11** did not afford CHN microanalysis values that were within ±0.4% of the calculated values.

To understand the solution structures of adducts **1**-**3**, variable temperature ^1H NMR spectra were recorded for the diamagnetic Y complexes **3** and **6** in toluene-d_8 (Figures S15, S16). The behavior of **6** was determined first. At 20 °C, sharp singlets were observed at δ 4.52 (C-H), 2.39 (NMe_2), and 1.20 (tBu). The ^1H NMR spectrum at 60 °C revealed sharp singlets at δ 4.52 (C-H), 2.40 (NMe_2), and 1.17 (tBu), which are essentially identical to the chemical shifts at 20 °C. Upon cooling to -60 °C, the spectrum was very similar to those at 20 and 60 °C, with chemical shifts at δ 4.55 (C-H), 2.36 (NMe_2), and 1.31 (tBu). The solid state structure of **6** was not determined because X-ray quality crystals could not be grown, but it is likely a monomer (by analogy with **8**) or a dimer (by analogy with **7**). Observation of sharp resonances between -60 to 60 °C and minor chemical shift changes with temperature are consistent either with a monomeric structure or a dimeric structure where the exchange rate between the bridging and terminal L^1 ligands is rapid on the NMR timescale. The variable temperature ^1H NMR spectra of **3** were explored next. At 20 °C in toluene-d_8, **3** exhibited resonances at δ 4.52 (C-H), 2.39 (NMe_2), and 1.21 (tBu) for the L^1 ligands and at δ 3.01 (CH_2), 2.21 (NMe_2), and 0.95 (tBu) for the L^1H ligand. The L^1:L^1H integration was 3:1. Interestingly, the L^1 resonances in **3** at 20 °C had exactly the same chemical shifts as **6** at the same temperature. Moreover, the chemical shifts of

pure L^1H in toluene-d_8 at 20 °C (δ 2.98 (CH_2), 2.16 (NMe_2), and 0.96 (tBu)) were very close to those exhibited by the L^1H ligand in **3** at 20 °C. These chemical shift values suggest that L^1H is weakly bound to the Y ion in **3** at 20 °C and that the equilibrium **3** ↔ **6** + L^1H lies to the right under these conditions. Increasing the temperature to 60 °C led to resonances at δ 4.52 (C-H), 2.40 (NMe_2), and 1.16 (tBu) for the L^1 ligands and at δ 2.99 (CH_2), 2.18 (NMe_2), and 0.98 (tBu) for the L^1H ligand. These chemical shifts are essentially identical to those observed at 20 °C. The ^1H NMR spectrum at -60 °C consisted of three *tert*-butyl resonances at δ 1.49, 1.37, and 0.67, in a 2:1:1 ratio. The resonance at δ 0.67 arose from the L^1H ligand and showed an upfield shift of δ 0.28 upon cooling from 20 to -60 °C. The resonances at δ 1.49 and 1.37 existed as a single resonance at δ 1.39 at -40 °C and coalesced to the two resonances at -50 °C. The NMe_2 resonances at -60 °C consisted of a sharp resonance at δ 2.68 and broad resonances at δ 2.60 and 2.44. These resonances overlapped too much to allow an accurate relative integration. The enolate C-H resonance appeared at -60 °C as a slightly asymmetric singlet at δ 4.63. Taken together, the ^1H NMR spectrum of **3** at -60 °C is consistent with the solid state structure described below and shown in equation 1, since this structure would exhibit three *tert*-butyl resonances in a 2:1:1 ratio. Upon warming above -50 °C, the rate of exchange between the κ^2-L^1 and κ^1-L^1 ligands becomes rapid on the NMR timescale and only a single *tert*-butyl resonance is observed for the L^1 ligands. The L^1H ligand retains separate resonances over the -60 to 60 °C temperature range.

X-Ray Crystal Structures of 1-3, 7-9, 13, and 14. X-ray crystal structures were determined for **1**-**3**, **7**-**9**, **13**, and **14** to understand the molecular structures. The data for **9** were of lower resolution and are not discussed herein, but were sufficient to establish the overall dimeric structure and ligand connectivity. Crystallographic data are summarized in Tables S1-S3. Figures 1-7 show representative perspective views of **1**-**3**, **7**, **8**, **13**, and **14**, as well as selected bond lengths and angles. Single crystals of sufficient quality for structure determinations could not be obtained for **4**-**6**, **10**-**12**, and **15**.

Complex **1** crystallizes as an 8-coordinate monomer with three κ^2-L^1 ligands and one κ^2-L^1H ligand bonded to the Pr ion (Figure 1). The κ^2-L^1 ligands are characterized by Pr-O bond distances of 2.332(3), 2.309(3), and 2.44(1) Å and Pr-N bond lengths of 2.846(4), 2.739(4), and 2.84(2) Å. The longer Pr-O1C distance may reflect steric crowding about the 8-coordinate Pr ion. By contrast, the Pr-N distances fall within a narrow range of 2.74 to 2.85 Å. The κ^2-L^1H ligand has Pr-O and Pr-N bond lengths of 2.43(1) and 2.79(2) Å. The Pr-O4 distance is identical to that of Pr-O3 within experimental error. The Pr-N bond length is within the same range as those observed for the κ^2-L^1 ligands. The enolate C-C distances within the ligand backbones allow unambiguous assignment of the L^1 and L^1H ligands. Thus, the C1A-C2A, C1B-C2B, and C1C-C2C bond lengths are 1.339(7), 1.352(7), and 1.38(8) Å, and are close to the value expected for a C-C double bond (~1.32 Å). By con-

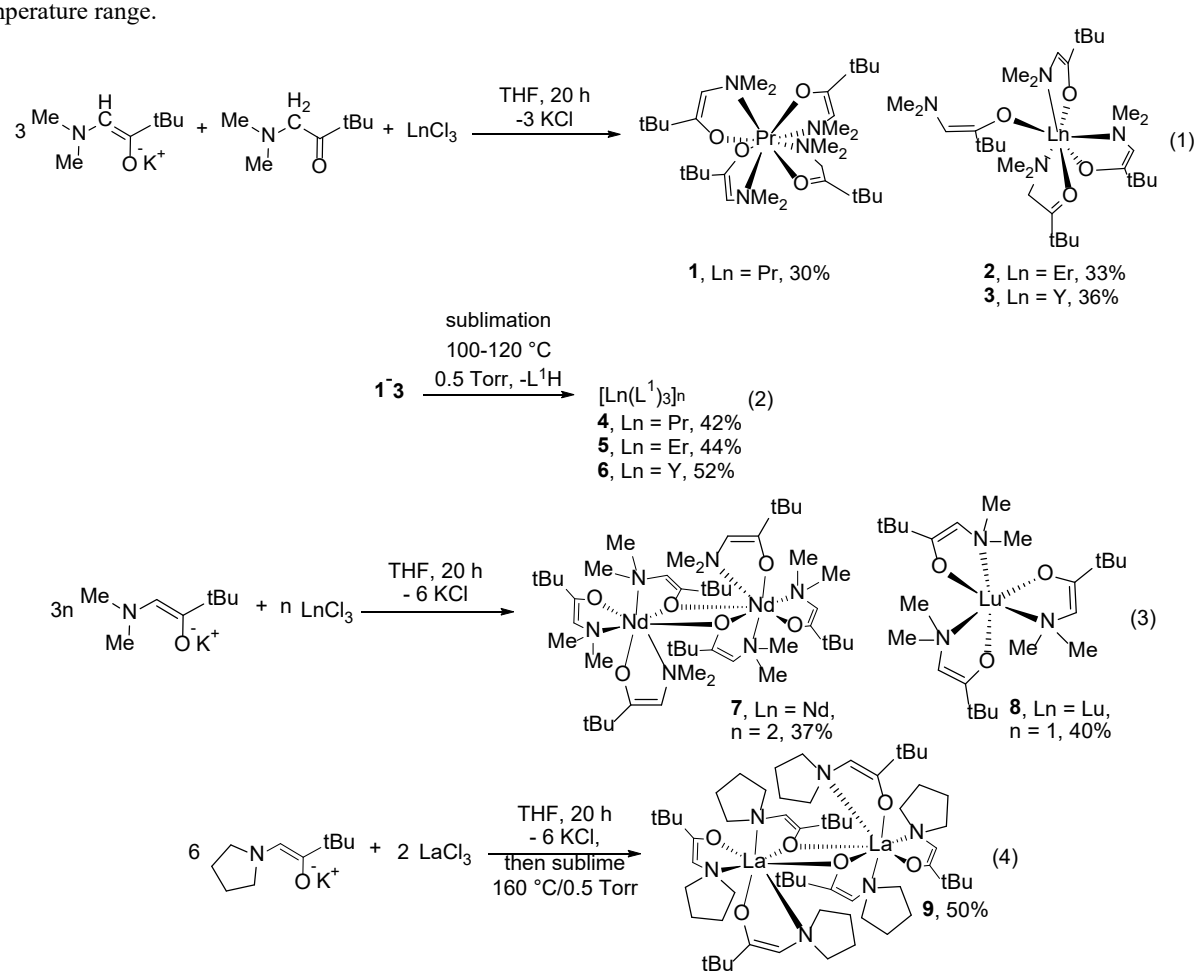

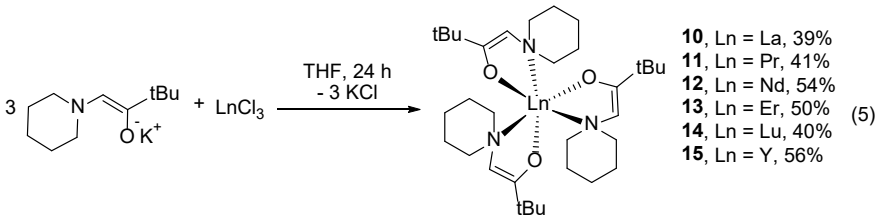

10, Ln = La, 39%
11, Ln = Pr, 41%
12, Ln = Nd, 54%
13, Ln = Er, 50%
14, Ln = Lu, 40%
15, Ln = Y, 56%
(5)

trast, the C1D-C2D distance is 1.47(2) Å, which is in the range for a C-C single bond.

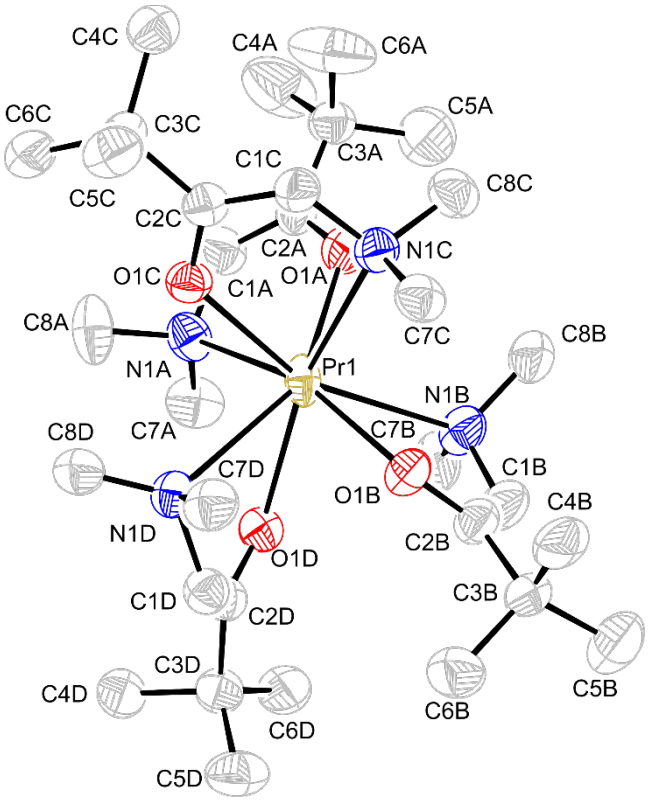

Figure 1. Perspective view of **1** with thermal ellipsoids at the 50% level. Selected bond lengths (Å) and angles (°): Pr-O1A 2.332(3), Pr-O1B 2.309(3), Pr-O1C 2.44(1), Pr-O1D 2.43(1), Pr-N1A 2.846(4), Pr-N1B 2.739(4), Pr-N1C 2.84(2), Pr-N1D 2.79(2), C1A-C2A 1.339(7), C1B-C2B 1.352(7), C1C-C2C 1.38(2), C1D-C2D 1.47(2); O1A-Pr-O1B 124.9(1), O1A-Pr-O1C 88.6(3), O1A-Pr-O1D 124.9(3), O1B-Pr-O1C 116.6(3), O1B-Pr-O1D 83.2(3), O1C-Pr-O1D 122.6(5), O1A-Pr-N1A 63.6(1), O1A-Pr-N1B 75.7(1), O1A-Pr-N1C 75.7(4), O1A-Pr-N1D 153.3(3), O1B-Pr-N1A 156.6(1), O1B-Pr-N1B 64.7(1), O1B-Pr-N1C 75.7(3), O1B-Pr-N1D 79.5(3), O1C-Pr-N1A 83.5(3), O1C-Pr-N1B 159.2(3), O1C-Pr-N1C 61.8(4), O1C-Pr-N1D 68.9(4), O1D-Pr-N1A 75.4(3), O1D-Pr-N1B 78.0(3), O1D-Pr-N1C 157.1(4), O1D-Pr-N1D 62.6(4), N1A-Pr-N1B 101.1(1), N1A-Pr-N1C 100.5(4), N1A-Pr-N1D 98.5(3), N1B-Pr-N2C 100.5(4), N1B-Pr-N2D 129.3(3), N1C-Pr-N1D 104.1(5).

Complex **2** crystallizes as a 7-coordinate monomer that contains two κ^2-L^1 ligands, one oxygen-bound κ^1-L^1 ligand, and one κ^2-L^1H ligand (Figure 2). The lower coordination number of **2**, compared to **1**, is consistent with the smaller ionic radius of the Er^{3+} ion (0.890 Å) relative to the Pr^{3+} ion (0.990 Å).[58] The *tert*-butyl and dimethylamino groups are anti with respect to each other across the enolate C=C bond in the κ^1-L^1 ligand. The κ^2-L^1 ligands have Er-O bond distances of 2.183(2) and 2.200(2) Å and Er-N bond distances of 2.559(2) and 2.619(2) Å. The κ^1-L^1 ligand has an Er-O distance of 2.121(2) Å, and is shorter than the related distances for the κ^2-L^1 ligands because of lower steric interactions. The Er-N distance is 4.594(2) Å for the κ^1-L^1 ligand and is clearly not a bonding interaction. The κ^2-L^1H ligand has Er-O and Er-N distances of 2.446(2) and 2.592(2) Å, respectively. The C-C distances within the L^1 ligand backbones are 1.331(4), 1.334(4), and 1.338(4) Å, which are consistent with C-C double bonds that are expected for enolate ligands. By contrast, the C-C distance for the L^1H ligand is 1.502(4) Å, which is in the range for a C-C single bond.

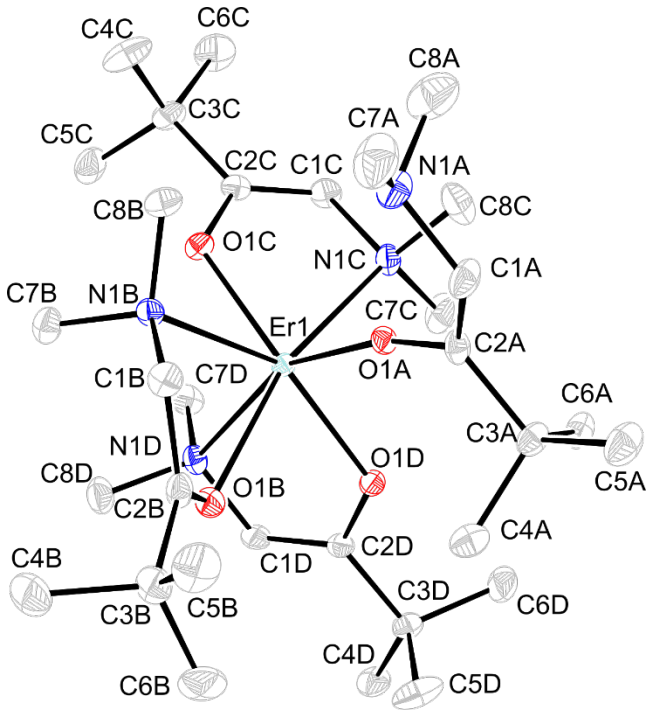

Figure 2. Perspective view of **2** with thermal ellipsoids at the 50% level. Selected bond lengths (Å) and angles (°): Er-O1A 2.121(2), Er-O1B 2.446(2), Er-O1C 2.200(2), Er-O1D 2.183(2), Er-N1B 2.592(2), Er-N1C 2.559(2), Er-N1D 2.619(2), C1A-C2A 1.331(4), C1B-C2B 1.502(4), C1C-C2C 1.338(4), C1D-C2D 1.334(4); O1A-Er-O1B 86.63(7), O1A-Er-O1C 121.07(7), O1A-Er-O1D 91.62(7), O1B-Er-O1C 123.75(6), O1B-Er-O1D 81.52(6), O1C-Er-O1D 137.06(7), O1A-Er-N1B 80.89(7), O1A-Er-N1C 89.76(7), O1A-Er-N1D 157.31(7), O1B-Er-N1B 63.58(6), O1B-Er-N1C 166.00(7), O1B-Er-N1D 81.52(6), O1C-Er-N1D 137.06(7), N1B-Er-N1C 129.12(7), N1B-Er-N1D 107.65(7), N1C-Er-N1D 99.92(7).

Complex **3** adopts a 7-coordinate structure that is very similar to that of **2**, with two κ^2-L^1 ligands, one oxygen-bound κ^1-L^1 ligand, and one κ^2-L^1H ligand (Figure 3). Like **2**, the *tert*-butyl and dimethylamino groups are anti with respect to each other across the enolate C=C bond in the κ^1-L^1 ligand. The structural similarities of **2** and **3** are not surprising, given the similar ionic radii of Er^{3+} (0.890 Å) and Y^{3+} (0.900 Å).[58] The κ^2-L^1 ligands have Y-O bond distances of 2.206(1) and 2.187(1) Å and Y-N bond distances of 2.579(2) and 2.633(2) Å. The κ^1-L^1 ligand has an Y-O distance of 2.128(1) Å, and is shorter than the related distances for the κ^2-L^1 ligands because of lower steric interactions. The non-bonding Y-N distance is 4.604(2) Å for the κ^1-L^1 ligand and is identical to the related value in **2**. The κ^2-L^1H ligand has Y-O and Y-N distances of 2.457(1) and 2.612(2) Å, respectively. The C-C distances within the L^1 ligand backbones are 1.337(3), 1.335(3), and 1.335(3) Å, which are identical to the values in **2** and are consistent with C-C enolate double bonds. The C-C single bond distance for the L^1H ligand is 1.501(3) Å, which is identical to the value in **1** and **2**.

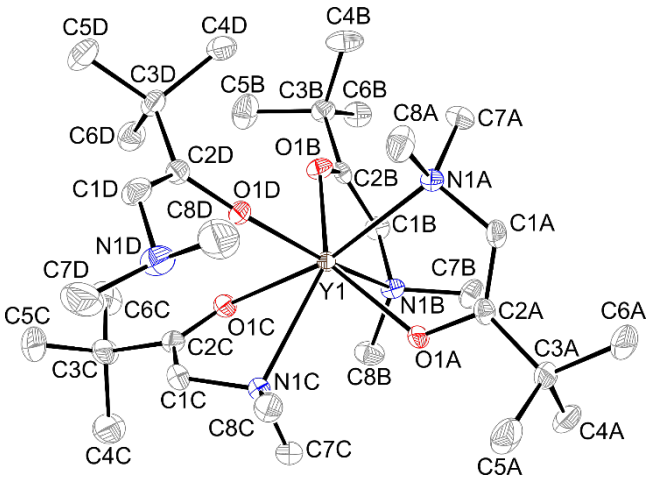

Figure 3. Perspective view of **3** with thermal ellipsoids at the 50% level. Selected bond lengths (Å) and angles (°): Y-O1A 2.206(1), Y-O1B 2.187(1), Y-O1C 2.457(1), Y-O1D 2.128(1), Y-N1A 2.579(2), Y-N1B 2.633(2), Y-N1C 2.612(2), C1A-C2A 1.337(3), C1B-C2B 1.335(3), C1C-C2C 1.501(3), C1D-C2D 1.335(3); O1A-Y-O1B 136.64(5), O1A-Y-O1C 123.80(5), O1A-Y-O1D 120.81(5), O1B-Y-O1C 81.93(5), O1B-Y-O1D 92.08(5), O1C-Y-O1D 86.70(5), O1A-Y-N1A 69.05(5), O1A-Y-N1B 81.88(5), O1A-Y-N1C 73.38(5), O1B-Y-N1A 85.07(6), O1B-Y-N1B 68.66(5), O1B-Y-N1C 144.84(5), O1C-Y-N1A 166.39(5), O1C-Y-N1B 79.01(5), O1C-Y-N1C 63.39(5), O1D-Y-N1A 89.78(6), O1D-Y-N1B 157.31(5), O1D-Y-N1C 80.88(5), N1A-Y-N1B 99.97(6), N1A-Y-N1C 128.95(6), N1B-Y-N1C 107.65(6).

Complex **7** adopts a dimeric structure that contains two L^1 ligands that bridge between the Nd ions through the oxygen atoms, and then two κ^2-L^1 ligands that are bonded to each Nd ion (Figure 4). Each Nd ion is 7-coordinate. The Nd1-Nd2 distance is 4.0205(7) Å. The bridging L^1 ligands are characterized by Nd-O distances of 2.410(5), 2.470(6), 2.466(6), and 2.455(5) Å. These values are essentially identical, although the Nd1-O1 distance may differ slightly from the Nd1-O4 distance within experimental uncertainty. The Nd-N bond lengths associated with the bridging L^1 ligands are 2.595(7) and 2.610(7) Å. The Nd-O bond lengths for the terminal κ^2-L^1 ligands are 2.241(5), 2.256(8), 2.266(5), and 2.244(5) Å. These values are shorter than those for the bridging L^1 ligands, as expected. The Nd-N bond distances for the terminal κ^2-L^1 ligands are 2.852(9), 2.93(1), 2.819(7), and 2.848(7) Å. Interestingly, these values are 0.20 to 0.35 Å longer than those associated with the bridging L^1 ligands, which may arise from greater steric interactions upon forming Nd-N bonds in the terminal κ^2-L^1 ligands. The enolate C-C distances within the L^1 ligand backbones fall within the narrow range of 1.32(1) to 1.33(2) Å, which are consistent with double bonds and are similar to the values in the L^1 ligands of **1**-**3**.

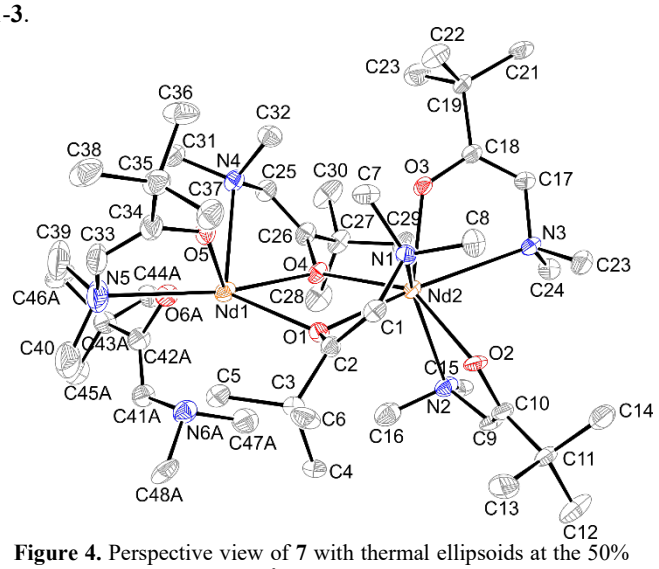

Figure 4. Perspective view of **7** with thermal ellipsoids at the 50% level. Selected bond lengths (Å) and angles (°): Nd1-Nd2 4.0205(7), Nd1-O1 2.410(5), Nd1-O4 2.470(6), Nd1-O5 2.241(5), Nd1-O6A 2.256(8), Nd2-O1 2.466(6), Nd2-O2 2.266(5), Nd2-O3 2.244(5), Nd2-O4 2.455(5), Nd1-N4 2.610(7), Nd1-N5 2.852(9), Nd1-N6A 2.928(2), Nd2-N1 2.595(7), Nd2-N2 2.819(7), Nd2-N3 2.848(7), C1-C2 1.33(1), C9-C10 1.32(1), C17-C18 1.33(1), C25-C26 1.33(1), C33-C34 1.33(1), C41A-C42A 1.33(2); O1-Nd1-O4 68.4(2), O1-Nd1-O5 88.0(2), O1-Nd1-O6A 94.3(2), O1-Nd2-O2 90.1(2), O1-Nd2-O3 118.3(2), O1-Nd2-O4 67.8(2), O4-Nd1-O5 119.8(2), O4-Nd1-O6A 92.9(3), O5-Nd1-O6A 75.4(3), O1-Nd2-O2 90.1(2), O1-Nd2-O3 118.3(2), O1-Nd2-O4 67.8(2), O2-Nd2-O3 129.9(2), O2-Nd2-O4 145.0(2), O3-Nd2-O4 85.1(2), Nd1-O1-Nd2 111.1(2), Nd1-O4-Nd2 109.4(2), O1-Nd1-N4 115.6(2), O1-Nd1-N5 125.8(2), O1-Nd1-N6A 94.3(2), O4-Nd1-N4 65.9(2), O4-Nd1-N5 165.7(2), O4-Nd1-N6A 103.3(3), O5-Nd1-N5 63.5(2), O5-Nd1-N6A 125.4(3), O6-Nd1-N6A 62.0(3), O1-Nd2-N1 65.5(2), O1-Nd2-N2 102.6(2), O1-Nd2-N3 164.4(2), N4-Nd1-N5 103.0(2), N4-Nd1-N6A 138.4(3), N5-Nd1-N6A 78.8(3), N1-Nd2-N2 140.8(2), N1-Nd2-N3 101.3(2), N2-Nd2-N3 82.1(2).

Complex **8** crystallizes as a 6-coordinate monomeric complex that contains three κ^2-L^1 ligands (Figure 5). The geometry about the Lu ion is distorted octahedral. The lower coordination number in **8**, relative to **1**-**3** and **7**, arises from the smaller size of the Lu^{3+} ion (0.861 Å),[58] relative to the other ions. The Lu-O bond lengths are 2.115(2), 2.132(2), and 2.129(2) Å, which are identical within experimental uncertainty. The Lu-N bond distances are 2.459(2), 2.530(2), and 2.470(2) Å. The N atoms associated with the two shorter Lu-N bond lengths are mutually trans within the coordination sphere, whereas the N atom associated with the slightly longer Lu-N1B distance is trans to an O atom. The more strongly bonded O atom is likely responsible for the slight lengthening of the Lu-N1B bond. The enolate C-C distances within the L^1 backbones are 1.330(4), 1.336(4), and

1.336(4) Å. These values are consistent with C-C double bonds and are identical to the related values observed in the L^1 ligands of **1**-**3** and **7**.

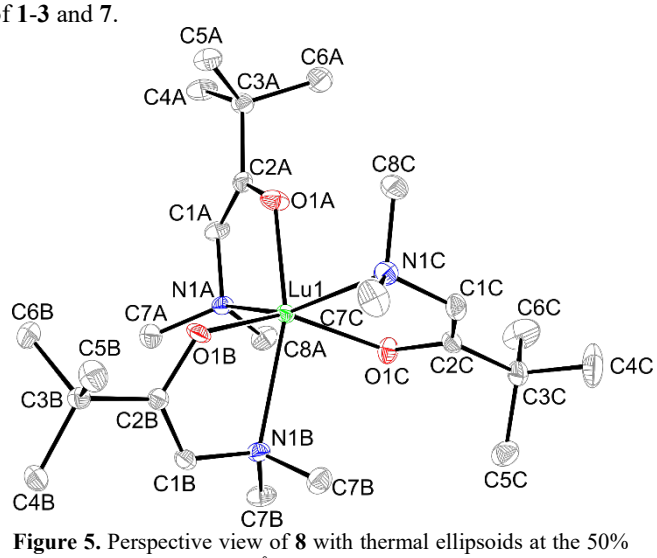

Figure 5. Perspective view of **8** with thermal ellipsoids at the 50% level. Selected bond lengths (Å) and angles (°): Lu-O1A 2.115(2), Lu-O1B 2.132(2), Lu-O1C 2.129(2), Lu-N1A 2.459(2), Lu-N1B 2.530(2), Lu-N1C 2.470(2), C1A-C2A 1.330(4), C1B-C2B 1.336(4), C1C-C2C 1.336(4); O1A-Lu-O1B 103.43(7), O1A-Lu-O1C 108.61(7), O1B-Lu-O1C 144.41(7), O1A-Lu-N1A 73.21(7), O1A-Lu-N1B 161.87(7), O1A-Lu-N1C 97.98(7), O1B-Lu-N1B 70.09(7), O1B-Lu-N1C 83.25(7), O1C-Lu-N1C 73.17(7), N1A-Lu-N1B 91.94(7), N1A-Lu-N1C 153.68(7), N1B-Lu-N1C 111.02(7).

Complex **13** crystallizes as a 6-coordinate monomer that contains three κ^2-L^3 ligands (Figure 6). The geometry about the Er ion is distorted octahedral. The 6-coordinate structure of **13** with three κ^2-L^3 ligands differs markedly from the 7-coordinate structure of **2**, which contains two κ^2-L^1 ligands, one oxygen-bound κ^1-L^1 ligand, and one κ^2-L^1H ligand. The molecular structure of **13** is clearly impacted strongly by the larger steric bulk of the piperidinyl substituent in L^3, compared to the dimethylamino group in L^1. The bulkier L^3 ligand blocks coordination of an L^3H ligand to the Er ion, but the L^3 ligand is not too bulky and three κ^2-L^3 ligands can be accommodated. The Er-O bond lengths are 2.150(5), 2.141(5), and 2.141(5) Å, which are identical within experimental uncertainty. The Er-N bond distances are 2.545(6), 2.615(6), and 2.532(6) Å. As described for **8**, the N atoms associated with the two shorter Er-N bond lengths, Er-N1A and Er-N3, are mutually trans within the coordination sphere, whereas N atom with the longer Er-N distances, Er-N2A, is trans to an O atom (O3). The stronger Er-O3 bond is likely responsible for the longer Er-N2A bond length. The enolate C-C distances within the L^3 ligand backbone are 1.315(9), 1.324 (9), and 1.317(9) Å. These values are consistent with double bonds and are identical to the values for **1**-**3**, **7**, and **8** within experimental uncertainty.

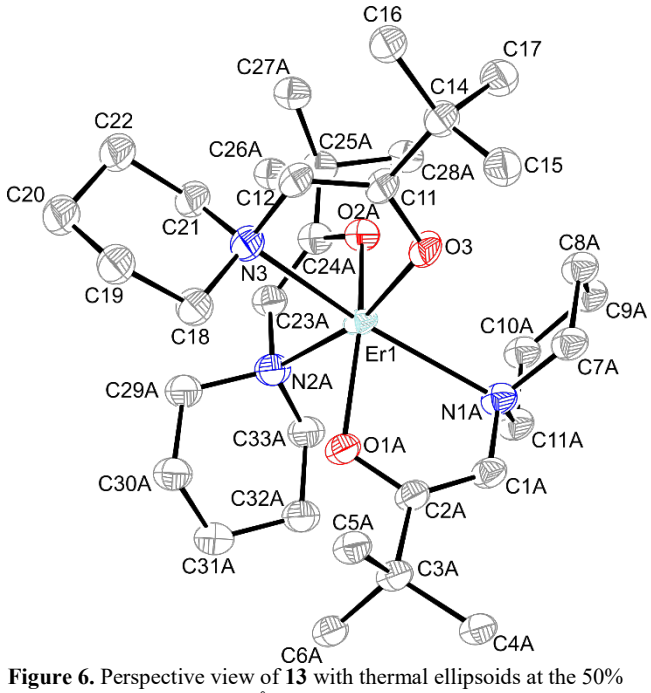

Figure 6. Perspective view of **13** with thermal ellipsoids at the 50% level. Selected bond lengths (Å) and angles (°): Er-O1A 2.150(5), Er-O2A 2.141(5), Er-O3 2.141(5), Er-N1A 2.545(6), Er-N2A 2.615(6), Er-N3 2.532(6), C1A-C2A 1.315(9), C23A-C24A 1.324(9), C11-C12 1.317(9); O1A-Er-O2A 151.8(3), O1A-Er-O3 107.4(3), O2A-Er-O3 100.0(3), O1A-Er-N1A 72.1(2), O1A-Er-N2A 85.3(3), O1A-Er-N3 99.8(2), O2A-Er-N2A 68.4(2), O2A-Er-N3 94.9(3), O3-Er-N3 72.0(2), N1A-Er-N2A 105.6(2), N1A-Er-N3 152.2, N2A-Er-N3 100.0(2).

Complex **14** adopts a 6-coordinate monomeric molecular structure that is very similar to those found in **8** and **13**. The Lu-O bond lengths are 2.139(5), 2.117(5), and 2.112(5) Å, which are identical within experimental uncertainty. The Lu-N bond distances are 2.479(7), 2.458(5), and 2.40(2) Å. These distances are also identical within experimental error. The enolate C-C distances within the L^3 ligand backbone are 1.36(1), 1.351(9), and 1.35(1) Å. These values are consistent with double bonds and are identical to the values for **1**-**3**, **7**, **8**, and **13** within experimental uncertainty.

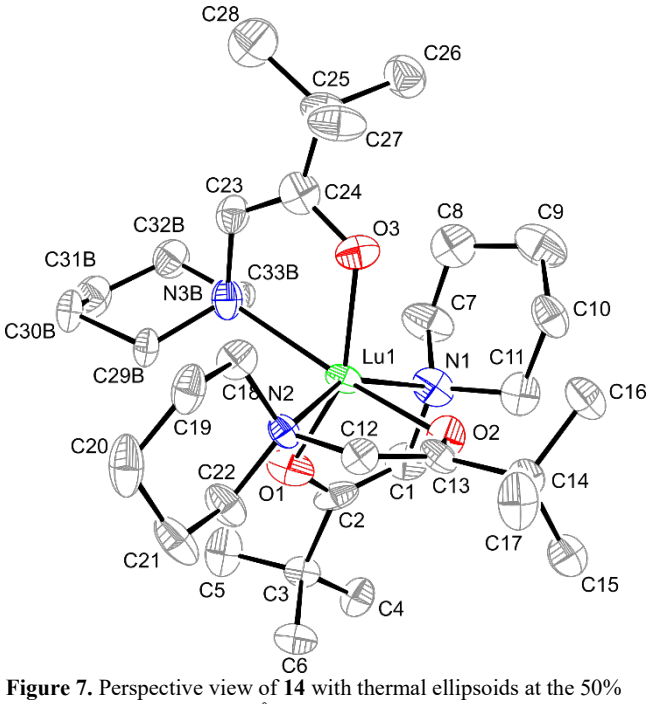

Figure 7. Perspective view of **14** with thermal ellipsoids at the 50% level. Selected bond lengths (Å) and angles (°): Lu-O1 2.139(5), Lu-O2 2.117(5), Lu-O3 2.112(5), Lu-N1 2.479(7), Lu-N2 2.458(5), Lu-N3B 2.40(2), C1-C2 1.36(1), C12-C13 1.351(9), C23-C24 1.35(1); O1-Lu-O2 107.8(2), O1-Lu-O3 150.5(2), O2-Lu-O3 101.1(2), O1-Lu-N1 74.0(2), O1-Lu-N2 98.2(2), O1-Lu-N3B 82.5(3), O2-Lu-N1 85.0(2), O2-Lu-N2 73.6(2), O2-Lu-N3B 167.1(5), O3-Lu-N3B 69.9(3), N1-Lu-N2 153.8(2), N1-Lu-N3B 105.7(7), N2-Lu-N3B 97.7(7).

Comparison of Structure Data with Related Complexes. Only a few examples of lanthanide complexes containing enolate-based ligands have been structurally characterized. A common feature of previously reported complexes is that the enolate moieties are part of more complex chelating ligands.[59-62] The C=C double bond lengths within the enolate fragments range from 1.33 to 1.37 Å.[59-62] These previously reported bond lengths are close to the values observed herein. A series of structurally characterized lanthanide(III) aryloxides provides Ln-O bond length comparisons with some of the complexes reported herein. The complexes $[Nd_2(O\text{-}C_6\text{-}2,4,6\text{-}Me_3H_2)_6(THF)_4]\bullet 2THF$ and $[Nd_2(O\text{-}C_6\text{-}2,4,6\text{-}Me_3H_2)_6(DME)_2]\bullet$toluene are dimeric with two bridging aryloxide ligands between the Nd ions and two terminal aryloxide ligands per Nd ion.[63] This dimeric structure is broadly similar to that of **7**. The bridging Nd-O bond lengths in $[Nd_2(O\text{-}C_6\text{-}2,4,6\text{-}Me_3H_2)_6(THF)_4]\bullet 2THF$ (2.410(2), 2.428(2) Å) and $[Nd_2(O\text{-}C_6\text{-}2,4,6\text{-}Me_3H_2)_6(DME)_2]\bullet$toluene (2.357(1), 2.500(1) Å) are similar to those observed in **7** (2.410(5), 2.470(6) Å). The terminal Nd-O bond distances in $[Nd_2(O\text{-}C_6\text{-}2,4,6\text{-}Me_3H_2)_6(THF)_4]\bullet 2THF$ (2.220(2), 2.216(2) Å) and $[Nd_2(O\text{-}C_6\text{-}2,4,6\text{-}Me_3H_2)_6(DME)_2]\bullet$toluene (2.204(2), 2.192(2) Å) are slightly shorter than the related values in **7** (2.241(5), 2.256(8), 2.266(5), 2.244(5) Å), consistent with a Nd ion coordination number of seven in **7** versus six in the Nd aryloxides. The complex $Er(O\text{-}C_6\text{-}2,4,6\text{-}Me_3H_2)_3(THF)_3$ has Er-O bond lengths of 2.082(6), 2.099(7), and 2.111(7) Å,[63] and can be compared to the related values in **2** and **13**. In **2**, the Er-O distances associated with the anionic L^1 ligands are 2.121(2), 2.200(2), and 2.183(2) Å. The shortest of these distances corresponds to the κ^1-L^1 ligand, and this value is similar to the values Er-O bond lengths in $Er(O\text{-}C_6\text{-}2,4,6\text{-}Me_3H_2)_3(THF)_3$. The two Er-O distances for the anionic κ^2-L^1 ligands are longer than the values in $Er(O\text{-}C_6\text{-}2,4,6\text{-}Me_3H_2)_3(THF)_3$, which likely arises from steric interactions associated with the bidentate coordination mode. The Er-O bond length for the κ^2-L^1H ligand in **2** is 2.446(2) Å, which is in the range for the Er-O bond lengths for the THF ligands in $Er(O\text{-}C_6\text{-}2,4,6\text{-}Me_3H_2)_3(THF)_3$ (2.434(7), 2.435(7) Å). The Er-O distances for the κ^2-L^3 ligands in **13** (2.150(5), 2.141(5), 2.141(5) Å) are longer than those in $Er(O\text{-}C_6\text{-}2,4,6\text{-}Me_3H_2)_3(THF)_3$, likely because of steric congestion in the coordination sphere caused by the piperidino substituents. Since the ionic radii of Er(III) and Y(III) are very similar, the Y-O bond length comparisons between $Er(O\text{-}C_6\text{-}2,4,6\text{-}Me_3H_2)_3(THF)_3$[63] and **3** are very close to those described above for $Er(O\text{-}C_6\text{-}2,4,6\text{-}Me_3H_2)_3(THF)_3$ and **2**. The reported crystal structures of $Pr(O\text{-}C_6H_3\text{-}2,6\text{-}iPr_2)_3(THF)_2$ and $Lu(O\text{-}C_6H_3\text{-}2,6\text{-}iPr_2)_3(THF)_2$ offer bond length comparisons with **1**, **8**, and **14**.[64] The Pr-O aryloxide bond lengths in $Pr(O\text{-}C_6H_3\text{-}2,6\text{-}iPr_2)_3(THF)_2$ are 2.142(8), 2.158(9), and 2.216(9) Å, which are shorter than those observed for the κ^2-L^1 ligands in **1** (2.332(3), 2.309(3), 2.44(1) Å). The Pr-O bond distance for the κ^2-L^1H in **1** is 2.43(1) Å. The coordination numbers in $Pr(O\text{-}C_6H_3\text{-}2,6\text{-}iPr_2)_3(THF)_2$ and **1** are five and eight, respectively, which account for the differing Pr-O bond lengths. The Lu-O aryloxide bond lengths in $Lu(O\text{-}C_6H_3\text{-}2,6\text{-}iPr_2)_3(THF)_2$ (2.041(4), 2.042(3), 2.048(4) Å) are also shorter than the related values in **8** (2.115(2), 2.129(2), 2.132(2) Å) and **14** (2.112(5), 2.117(5), 2.139(5) Å). The coordination number of five in $Lu(O\text{-}C_6H_3\text{-}2,6\text{-}iPr_2)_3(THF)_2$ is less crowded, compared to the coordination number of six in **8** and **14**.

The Ln-N bond lengths in **1**-**3**, **7**-**9**, **13**, and **14** can be compared with selected complexes of similar coordination numbers containing the 1,10-phenanthroline (phen) ligand. The phen ligand was chosen as an analog of the NR_2 fragments in L^1 and L^3 ligands, since all are neutral donors and because there are sufficient previously reported structures containing phen ligands to compare with the structures herein. The Pr-N bond lengths in $Pr(acac)_3(phen)$ (acac = 2,4-pentanedionate) are 2.659(5) and 2.690(6) Å,[65] which are shorter than the related values in **1** (2.739(4), 2.79(2), 2.84(2), 2.846(4) Å), although the differences are at the edge of experimental uncertainty. The longer Pr-N distances in **1** may reflect increased steric crowding due to accommodation of the NMe_2 groups, relative to the situation with the phen ligand in $Pr(acac)_3(phen)$. The Nd-N bond lengths in eight-coordinate $Nd(pfnp)_3(phen)$ (pfnp = 4,4,5,5,5-pentafluoro-1-(2-napthyl)-1,3-butanedionate) range between 2.61 and 2.67 Å,[66] which are similar to the shortest Nd-N bond lengths in **7** (2.610(7), 2.595(7) Å). The longer Nd-N bond lengths in **7** (2.82 to 2.93 Å) probably reflect considerable steric crowding the coordination spheres of the Nd ions. The Er-N bond distances in $Er(pfnp)_3(phen)$[66] are between 2.49 and 2.55 Å, which are similar to slightly shorter than the related values in **2** (2.592(2), 2.559(2), 2.619(2) Å) and **13** (2.532(6), 2.545(6), 2.615(6) Å), despite the coordination numbers of eight in $Er(pfnp)_3(phen)$ and seven and six in **2** and **13**, respectively. Again, the bulky nature of the L^1, L^1H, and L^3 ligands in **2** and **13** create steric congestion about the Er ions that likely leads to slight lengthening of the Er-N distances. The complex $Y(TTA)_3(phen)$ (TTA = 4,4,4-trifluoro-1-(2-thienyl)-1,3-butanedionate) has Y-N bond lengths of 2.535(6) and 2.558(5) Å,[67]

which are similar to slightly shorter than the analogous values found in seven-coordinate **3** (2.579(2), 2.612(2), 2.633(2) Å). The slightly longer Y-N bond lengths in **3**, compared to $Y(TTA)_3(phen)$, are likely attributed to the steric congestion about the Y ion that occurs through coordination of the L^1 and L^1H NMe_2 groups. The eight-coordinate complex $Lu(acac)_3(phen)$ has Lu-N bond distances of 2.50(2) and 2.521(6) Å,[68] which are similar to slightly longer than the Lu-N values in six-coordinate **8** (2.459(2), 2.470(2), 2.530(2) Å) and **14** (2.40(2), 2.458(5), 2.479(7) Å). The slightly longer Lu-N distances in $Lu(acac)_3(phen)$, compared to **8** and **14**, can be attributed to the differences in coordination numbers of these complexes.

Precursor Properties. Melting point determinations, preparative sublimations, decomposition temperature measurements, and thermogravimetric analyses (TGA) were carried out to determine the suitability of **1**-**15** for use as ALD precursors. Details of these measurements are given in the Experimental Section and Supporting Information. Table 1 summarizes the melting point and sublimation and decomposition temperatures for **1**-**15**.

Liquid precursors in ALD are highly desirable, because the surface areas of liquids are constant, thereby leading to constant gas phase precursor concentrations. By contrast, the surface areas of solid precursors may not be constant during vapor transport, which may afford gas phase precursor concentrations that change with precursor loading. Among **1**-**15**, **2**, **5**, **7**, **10**-**12**, and **15** have melting points that are lower than their sublimation temperatures and thus undergo vapor transport from the liquid state.

Clear trends are apparent in the sublimation temperatures. The complexes containing L^1 ligands (**1**-**8**) sublime at the lowest temperatures among the series, likely because they have the lowest molecular weights. Complexes **1**-**3** sublime with loss of L^1H between 100 and 120 °C, and these sublimation temperatures are the same as those exhibited by **4**-**6**. Nd complex **7** is dimeric in the solid state, but sublimes at 120 °C at 0.5 Torr. Since **7** is a liquid at 120 °C, it is possible that there is a monomer-dimer equilibrium present and vapor transport may occur from the monomers. The dimeric La complex **9** has the highest sublimation temperature, which may arise from its dimeric structure and melting point that is higher than the sublimation temperature. Complexes **10**-**15** contain L^3 ligands, and sublime at 140-160 °C at 0.5 Torr. These higher sublimation temperatures likely occur because the L^3 complexes have the highest molecular weights among the monomeric complexes.

Decomposition temperatures were determined in sealed capillary tubes containing a few milligrams of **1**-**15** that were heated at 5 °C per minute until a color change to orange or red was observed. Complexes containing L^3 ligands (**10**-**15**) showed the highest decomposition temperatures (255-290 °C), while the dimeric La complex **9** containing L^2 ligands decomposed at 180 °C. Complexes containing L^1 ligands (**1**-**8**) exhibited intermediate thermal stabilities (180-265 °C). The thermal stability trends may arise from differences in the steric bulk of the ligand substituents. Complexes containing the L^3 ligand may be large enough to protect the metal ions from intramolecular and intermolecular decomposition reactions better than complexes containing L^1 and L^2 ligands. Interestingly, decomposition temperatures of **1**-**3** in sealed capillary tubes were 8 to 46 °C lower than those of the analogous complexes **4**-**6** that do not contain L^1H. It is likely that the presence of L^1H in liquid **1**-**3** leads to decomposition at lower temperatures than for pure **4**-**6**.

Table 1. Melting points, sublimation temperatures, and decomposition temperatures for **1**-**15**.

	mp (°C)	Subl. Temp. at 0.5 Torr (°C)	Dec. Temp. (°C)
1, $Pr(L^1)_3(L_1H)$	128-130	120	206
2, $Er(L^1)_3(L_1H)$	107-110	110	229
3, $Y(L^1)_3(L_1H)$	120-123	100	180
4, $[Pr(L^1)_3]_n$	133-136	120	220
5, $[Er(L^1)_3]_n$	93-95	110	265
6, $[Y(L^1)_3]_n$	111-115	100	188
7, $[Nd(L^1)_3]_2$	73-76	120	210
8, $Lu(L^1)_3$	112-116	95	255
9, $[La(L^2)_3]_2$	171	160	180
10, $La(L^3)_3$	140-144	155	255
11, $Pr(L^3)_3$	124-128	150	280
12, $Nd(L^3)_3$	144-148	160	280
13, $Er(L^3)_3$	155-158	140	290
14, $Lu(L^3)_3$	167-172	140	272
15, $Y(L^3)_3$	152-155	160	280

The thermal behavior and volatility of **1**-**15** were further investigated by TGA. Figure 8 shows the representative TGA plots for **1**-**6** and **13**-**15**. TGA traces for **7**-**12** are presented in the supporting information (Figures S32, S33). Table S4 lists the onsets of volatization and percent residual masses for **1**-**15**. The TGA traces of **1**-**3** show two-step weight losses, with the first weight loss of about 20% beginning at around 80 °C, consistent with evolution of loosely coordinated L^1H (Figure 8a). For comparison, the weight percentages of L^1H are 23.3% (**1**), 19.4% (**2**), and 21.7% (**3**). Another weight loss event occurs between 120 and 180 °C with non-volatile residues after heating to 500 °C of 15%, 19%, and 7% for **1**-**3**, respectively. The TGA traces of **4**-**6** show single-step weight losses starting at about 140 °C. Interestingly, the percent non-volatile residues for **4**-**6** upon reaching 500 °C are lower than those observed for **1**-**3** (e.g., non-volatile residues of **4** < **1**, **5** < **2**, **6** ≤ **3**). This observation is consistent with the lower decomposition temperatures of **1**-**3**, compared to **4**-**6** and is likely related to enhanced decomposition of **1**-**3** in the presence of L^1H. Complexes **13**-**15** show single step weight losses up to their decomposition temperatures (272 to 290 °C). The 50% weight loss temperatures for **13**-**15** (~260 to 280 °C) are more positive than those for **4**-**6** (~220

to 230 °C), suggesting lower volatility of **13**-**15**. This trend is consistent with the sublimation temperatures for **4**-**6** and **13**-**15** shown in Table 1. The TGA traces of **10**-**12** (Figure S33) are very similar to those of **13**-**15** shown in Figure 8b. The TGA traces of **7**-**9** also show single step weight losses (Figure S32), but the non-volatile residues (~20 to 30%) are higher than those of **1**-**6** and **10**-**15**.

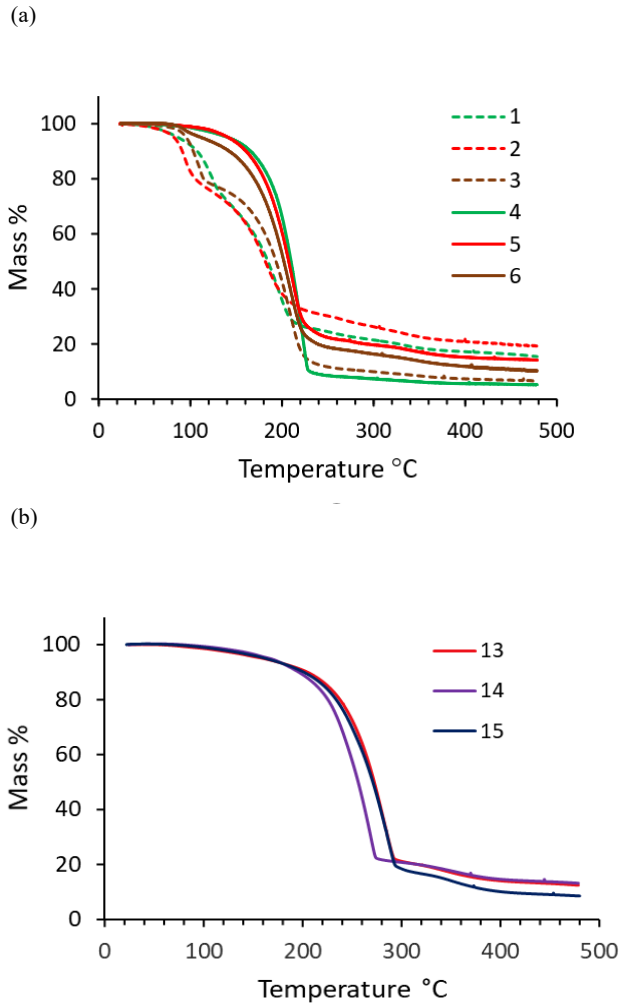

Figure 8. TGA traces of (a) L^1-containing complexes **1**-**6** and (b) L^3-containing complexes **13**-**15**.

The thermal stability of **6** was probed further by preparative sublimations. As noted above, sublimation of **3** gave a moderate yield of **6** (52%) and was accompanied by the formation of a non-volatile residue. A sample of **6** that was purified by sublimation was resublimed at 100 °C and 0.5 Torr, and afforded a 86% recovery of **6**. There was a small amount of non-volatile residue left after the sublimation, suggesting some decomposition during the vaporization process. Moreover, a 25 mg sample of **6** was sealed in a glass ampoule under argon and was heated in a furnace at 130 °C for 24 hours. The sample of **6** was initially a pale yellow solid, and became a red-orange oil after heating for 24 hours. ^{1}H NMR analysis (Figure S34) of the red-orange oil revealed a complex spectrum, of which the resonances for **6** were absent. Accordingly, **6** decomposed completely after heating at 130 °C for 24 hours and thus has low thermal stability at this temperature. It is likely that the L^1 ligand lacks sufficient steric bulk to protect the Ln-O and Ln-N bonds from decomposition reactions.

The decomposition temperatures shown in Table 1 demonstrate that the L^3-containing complexes **10**-**15** are more stable thermally than the remaining complexes **1**-**9** that contain L^1 or L^2 ligands. To provide further insights into long term stabilities, 25 mg samples of **10**-**15** were heated in sealed glass ampoules near their sublimation temperatures (140 °C for **13** and **14**, 150 °C for **10**-**12**, **15**) for 24 hours. The heated samples were analyzed by ^{1}H NMR spectroscopy for signs of decomposition (Figures S35-S41). The ^{1}H NMR spectra of **11**-**13** and **15** after 24 hours of heating were very similar to those prior to heating, suggesting that these complexes do not decompose under the heating conditions. Complexes **10** and **14** showed about 10-20% of free L^3H after 24 hours of heating, suggesting a small amount of decomposition. Accordingly, complexes containing the mid-sized Pr, Er, and Y ions have the highest thermal stabilities, whereas La^{3+} (largest ion) and Lu^{3+} (smallest ion) have slightly lower thermal stabilities. It is possible that the L^3 ligand has just the right steric profile to protect the Pr, Er, and Y ions from intramolecular and intermolecular reactions. The L^3 ligand may not be large enough to encapsulate the La^{3+} ion in **10** and may be too large for to fit around the Lu^{3+} ion in **14**. Accordingly, achieving the highest thermal stability for a given lanthanide ion will likely require "tuning" the ligand structures to obtain optimum steric interactions. Fortunately, analogs of L^1-L^3 can be easily prepared with alkyl and amino substituents of varying steric profiles.

Comparison of Precursor Properties with Previously Reported Lanthanide ALD Precursors. The L^3-containing complexes **10**-**15** are more stable thermally than **1**-**9**, which contain L^1 and L^2 ligands. However, the higher molecular weights of the L^3 ligands in **10**-**15**, relative to the ligands in **1**-**9**, lead to higher sublimation temperatures (140 to 160 °C at 0.5 Torr) than those found in L^1 complexes **1**-**8** (100 to 120 °C at 0.5 Torr). Complex **9** is dimeric, is the only complex containing L^2 ligands, and has a high sublimation temperature (160 °C at 0.5 Torr) and low decomposition temperature (180 °C).

Of the complexes reported here, **10**-**15** clearly have the best ALD precursor properties, because of their high thermal stabilities at the sublimation temperatures. It is difficult to compare the precursor properties of the compounds in the present work with those of precursors that have been previously used in the ALD of lanthanide-containing thin films, however, since precursor decomposition temperatures are rarely given. The decomposition temperature of a precursor is often close to the upper temperature limit of the ALD window in an ALD process.[69,70] This similarity can be used to perform an initial comparison of previous precursors with **10**-**15**.

Among previous lanthanide complexes, precursors containing β-diketonate or cyclopentadienyl ligands have been the most widely used.[29] Lanthanide complexes of the formula Ln(β-diketonate)$_3$ have very high thermal stabilities and can exhibit self-limited growth of oxides up to 400 °C.[4,29-32] However, Ln(β-diketonate)$_3$ precursors are unreactive toward water and require ozone as a co-reactant for oxide growth.[4,29-32] Ozone is highly reactive and causes oxidation of silicon substrates. Lanthanide cyclopentadienyl complexes also have very high thermal stabilities and water can be used as a co-reactant for the growth of oxide films.[29,33-36] For example, growth of Er_2O_3 films with $Er(C_5H_4Me)_3$ and water exhibits an ALD window from

about 250 to 350 °C on Si(100) substrates.[71] The growth of $PrAlO_3$ films using $Pr(C_5H_4iPr)_3$, $AlMe_3$, and water shows an ALD window from about 275 to 325 °C.[35] Accordingly, the thermal stabilities of lanthanide cyclopentadienyl precursors appears to be higher than those of **1**-**15**. However, the close similarity of the pKa values for water (pKa = 14.00, 15.7)[48] and cyclopentadiene (pKa = 16)[72] may lead to low reactivity of lanthanide cyclopentadienyl precursors with water in oxide growth. Moreover, ALD growth of some lanthanide cyclopentadienyl precursors with water do not exhibit self-limited growth.[73,74] Finally, the ALD growth of Pr_2O_3 films using $Pr(C_5H_4iPr)_3$ and ozone showed an ALD window from 200 to 250 °C, suggesting that not all lanthanide cyclopentadienyl precursors have high upper temperature limits for self-limited growth.[75] Precursors containing alkoxide, bis(trimethylsilylamide), and amidinate ligands have been evaluated as precursors for the growth of lanthanide oxide films, but exhibit problems that include lack of self-limiting growth, low decomposition temperatures, variable reactivity toward water, and impurity incorporation in the films.[29] Precursors containing new ligands such as guanidinate[40] and malonate[29] are promising. For example, ALD growth of Er_2O_3 using the guanidinate precursor $Er(iPrNC(NMe_2)NiPr)_3$ and water exhibited an ALD window from about 175 to 275 °C.[40] The upper limit of the ALD window for $Er(iPrNC(NMe_2)NiPr)_3$ is similar to the decomposition temperatures of **10**-**15** herein.

CONCLUSIONS

In this work, we have described the synthesis, molecular structures, volatilities, and thermal stabilities of lanthanide complexes **1**-**15** that contain enaminolate ligands. Among the structurally characterized complexes, **1**-**3**, **8**, **13**, and **14** have monomeric molecular structures, whereas **7** and **9** adopt dimeric structures. Complexes **1**-**15** are volatile, and sublime between 95 and 160 °C at 0.5 Torr. Complexes **1**-**8**, which contain NMe_2 groups in the L^1 ligand, sublime at the lowest temperatures (95 to 120 °C at 0.5 Torr), whereas complexes with L^2 (**9**) and L^3 ligands (**10**-**15**) sublime at 140 to 160 °C at 0.5 Torr. The trend of increasing sublimation temperatures (**1**-**8** < **9**-**15**) approximately follows the trend of increasing molecular weights for the monomeric complexes. Interestingly, the dimeric complexes **7** and **9** sublime at similar temperatures to the monomeric complexes, suggesting that the dimers may sublime as monomers. Complexes containing L^1 (**1**-**8**) and L^2 ligands (**9**) decompose in heated capillary tubes at temperatures between 180 and 265 °C, whereas the complexes with L^3 ligands (**10**-**15**) decompose between 255 and 290 °C. The higher thermal stabilities of **10**-**15** are attributed to the large steric bulk of the piperidinyl groups in L^3 ligands, which protects the lanthanide ions from intramolecular and intermolecular decomposition reactions better than the dimethylamino and pyrrolidinyl substituents in L^1 and L^2 ligands, respectively. Heating of **6** at 130 °C for 24 h led to complete decomposition, whereas similar treatment of **10**-**15** at their sublimation temperatures (140 to 150 °C) revealed a small amount of decomposition for **10** and **14** and no decomposition for **11**, **13**, and **15**. Accordingly, **10**-**15** have the best overall thin film precursor properties among the complexes described herein, in spite of their moderate sublimation temperatures (140-160 °C at 0.5 Torr). The use of **10**-**15** and related complexes in lanthanide oxide ALD film growth trials will be reported separately.

EXPERIMENTAL SECTION

General Considerations. All reactions and manipulations were carried out under an argon atmosphere using standard glovebox and Schlenk techniques, except that L^1H-L^3H ligands were synthesized in ambient atmosphere. Tetrahydrofuran and diethyl ether were distilled from purple solutions of sodium/benzophenone ketyl under an argon atmosphere. Hexane was distilled from sodium under an argon atmosphere. Anhydrous $LaCl_3$, $ErCl_3$, $LuCl_3$, and YCl_3 were purchased from Strem Chemicals, Inc. Anhydrous $PrCl_3$ and $NdCl_3$ were purchased from ProChem Inc. All of the anhydrous lanthanide chlorides were used as received. Potassium hydride (30 wt % dispersion in mineral oil) was purchased from Sigma-Aldrich and was washed with hexane before use. 1-Bromopinacolone was purchased from Combi-Blocks and triethylamine, dimethylamine, piperidine, and pyrrolidine were purchased from Sigma-Aldrich and were used as received. 1-(Dimethylamino)-3,3-dimethylbutan-2-one (L^1H),[76] 3,3-dimethyl-1-(pyrrolidin-1-yl)butan-2-one (L^2H),[76] and 3,3-dimethyl-1-(piperidin-1-yl)butan-2-one (L^3H)[77] were synthesized according to published procedures, except that diethyl ether was used as the reaction solvent for L^1H and L^2H, instead of benzene. Yields for **1**-**15** are based upon the amounts of lanthanide(III) chloride starting materials.

^1H and $^{13}C\{^1H\}$ NMR spectra were recorded using an Agilent 400 MHz spectrometer in benzene-d_6 or toluene-d_8, as indicated. All spectra were recorded at ambient temperature unless otherwise noted. Infrared spectra were measured using a Shimadzu IRTracer-100 spectrometer. Melting points and solid state thermal decomposition temperatures were determined using an Electrothermal-IA-9000 series digital melting point apparatus with a heating rate of 5 °C/min. TGA data were obtained using a TA instrument TGA Q-50 inside a nitrogen-filled glove box with a ramp of 10 °C/min. Elemental analyses were performed by Galbraith Laboratories, Inc., Knoxville, TN. We have previously described detailed procedures for decomposition temperature measurements and preparative sublimations.[78]

Preparation of $Pr(L^1)_3(L^1H)$ (1). A 100-mL Schlenk flask was charged with a magnetic stir bar, anhydrous $PrCl_3$ (0.432 g, 1.75 mmol), and tetrahydrofuran (10 mL). To this stirred solution at ambient temperature was slowly added a solution of KL^1 (prepared from L^1H (0.750 g, 5.25 mmol) and KH (0.231 g, 5.77 mmol) in tetrahydrofuran (25 mL)), followed by a solution of L^1H (0.250 g, 1.75 mmol) in tetrahydrofuran (5 mL). This solution was refluxed for 24 h. Upon cooling to room temperature, the volatile components were removed under reduced pressure and the resultant green-brown solid was dissolved in diethyl ether (40 mL). The solution was filtered through a 1-cm pad of Celite on a coarse glass frit and concentrated to about 15 mL under reduced pressure. The flask was then placed in a -30 °C freezer for 3 days. This procedure gave pale green X-ray quality crystals of **1** (0.375, 30%): mp 128-130 /°C, dec. 206 °C; IR (cm^{-1}) 2947 (m), 1682 (m), 1616 (m), 1333 (s), 1332 (s), 1132 (s), 1036 (m), 918 (m), 869 (m), 578 (m), 515 (w), 422 (m).

Anal. Calcd. for $C_{32}H_{65}PrN_4O_4$: C, 54.07; H, 9.22; N, 7.88. Found: C, 52.96; H 9.24; N 7.70.

Preparation of $Er(L^1)_3(L^1H)$ (2). In a fashion similar to the preparation of **1**, treatment of anhydrous $ErCl_3$ (0.478 g, 1.75 mmol) with a solution of KL^1 (prepared from L^1H (0.75 g, 5.25 mmol) and KH (0.231 g, 5.77 mmol)) was followed by addition of a solution of L^1H (0.250 g, 1.75 mmol). In contrast to **1**, the reaction mixture was stirred at ambient temperature instead of refluxing. Crystallization from diethyl ether afforded **2** as pale orange X-ray quality crystals (0.421 g, 33%): mp 107-110 °C, dec. 229 °C; IR (cm^{-1}) 2947 (m), 1678 (m), 1618 (m), 1454 (m), 1334 (s), 1136 (s), 1033 (m), 922 (m), 723 (m), 694 (m), 590 (m), 465 (m).

Anal. Calcd. for $C_{32}H_{65}ErN_4O_4$: C, 52.14; H, 8.89; N, 7.60. Found: C, 50.42; H, 8.64; N, 7.25.

Preparation of $Y(L^1)_3(L^1H)$ (3). In a fashion similar to the preparation of **2**, treatment of anhydrous YCl_3 (0.342 g, 1.75 mmol) with a solution of KL^1 (prepared from L^1H (0.75 g, 5.25 mmol) and KH (0.231 g, 5.77 mmol)), followed by a solution of L^1H (0.250 g, 1.75 mmol) afforded **3** (0.412 g, 36%) as yellow crystals from diethyl ether: mp 120-123 °C, dec. 180 °C; ^{1}H NMR (benzene-d_6, 23 °C, δ) 4.55 (br s, 3 H, C***H***), 3.05 (br s, 2 H, C***H***$_2$), 2.39 (br s, 18 H, N(C***H***$_3$)$_2$), 2.24 (br s, 6 H, N(C***H***$_3$)$_2$), 1.25 (br s, 27 H, C(C***H***$_3$)$_3$), 0.94 (br s, 9 H, C(C***H***$_3$)$_3$); ^{13}C{^{1}H} NMR (benzene-d_6, 23 °C, ppm) 167.00 (s, ***C***-O), 109.80 (s, ***C***HN), 63.63 (br s, N(***C***H$_3$)$_2$), 47.82 (s, N(***C***H$_3$)$_2$), 45.48 (s, ***C***H$_2$N), 43.40 (s, ***C***(CH$_3$)$_3$), 35.56 (s, ***C***(CH$_3$)$_3$), 28.75 (br s, C(***C***H$_3$)$_3$), 26.47 (br s, C(***C***H$_3$)$_3$); IR (cm^{-1}) 2945 (m), 1680 (m), 1618 (m), 1450 (m), 1337 (s), 1138 (s), 922 (m), 869 (m), 723 (m), 696 (m), 590 (m), 521 (m), 430 (m).

Anal. Calcd. for $C_{32}H_{65}YN_4O_4$: C, 58.34; H, 9.94; N, 8.50. Found: C, 57.23; H, 9.98; N, 8.29.

Preparation of $Pr(L^1)_3$ (4). A 0.300 g sample of **1** was placed in a 1 cm diameter glass tube and sublimed under reduced pressure (0.5 Torr) at 120 °C to afforded **4** as a pale green solid (0.101 g, 42%): mp 133-136 °C, dec. 220 °C; ^{1}H NMR (benzene-d_6, 23 °C, δ) 15.96 (br s), 9.55 (s), 6.74 (br s), -4.03 (br s), -22.49 (br s), -29.10 (br s); IR (cm^{-1}) 2949 (m), 1616 (w), 1458 (m), 1332 (s), 1134 (s), 1110 (m), 1041 (m), 918 (m), 867 (m), 581 (m), 424 (m).

Anal. Calcd. for $C_{24}H_{48}N_3O_3Pr$: C, 50.78; H, 8.52; N, 7.40. Found: C, 49.70; H, 8.78; N, 7.19.

Preparation of $Er(L^1)_3$ (5). Similar to the preparation of **4**, sublimation of 0.400 g of **2** at 110 °C/0.5 Torr afforded **5** as pale orange solid (0.142 g, 44%): mp 93-95 °C, dec. 265 °C; ^{1}H NMR (benzene-d_6, 23 °C, δ) 113.84 (br s), -47.83 (br s), -54.34 (br s); IR (cm^{-1}) 2947 (m), 1618 (m), 1454 (m), 1335 (s), 1136 (s), 1004 (m), 922 (m), 866 (w), 723 (m), 590 (m), 426 (m).

Anal. Calcd. for $C_{24}H_{48}ErN_3O_3$: C, 48.53; H, 8.15; N, 7.08. Found: C, 47.25; H, 8.33; N, 6.95.

Preparation of $Y(L^1)_3$ (6). In a fashion similar to the preparation of **4,** sublimation of 0.400 g of **3** at 100 °C/0.5 Torr afforded **6** as a pale yellow solid (0.162 g, 52%): mp 111–115 °C, dec. 188 °C; ^{1}H NMR (benzene-d_6, 23 °C, δ) 4.55 (s, 3 H, C***H***), 2.40 (s, 18 H, N(C***H***$_3$)$_2$), 1.25 (s, 27 H, C(C***H***$_3$)$_3$); ^{13}C{^{1}H} NMR (benzene-d_6, 23 °C, ppm) 167.17 (s, ***C***-O), 109.62 (s, ***C***HN), 47.69 (s, N(***C***H$_3$)$_2$), 35.49 (s, ***C***(CH$_3$)$_3$), 28.66 (s C(***C***H$_3$)$_3$); IR (cm^{-1}) 2945 (m), 1618 (m), 1452 (m), 1336 (s), 1138 (s), 1002 (m), 923 (m), 866 (m).

Anal. Calcd. for $C_{24}H_{48}N_3O_3Y$: C, 55.91; H, 9.38; N, 8.15. Found: C, 54.67; H, 9.42; N, 8.02.

Preparation of $[Nd(L^1)_3]_2$ (7). A 100-mL Schlenk flask was charged with a magnetic stir bar, anhydrous $NdCl_3$ (0.584 g, 2.33 mmol), and tetrahydrofuran (20 mL). To this stirred solution at ambient temperature was slowly added a solution of KL^1 (prepared in situ from L^1H (1.000 g, 6.98 mmol) and KH (0.336 g, 8.38 mmol)) in tetrahydrofuran (30 mL). This solution was refluxed for 20 h. The volatile components were removed under reduced pressure and the resultant pale blue-colored solid was subjected to sublimation at 120 °C/0.5 Torr to afford **7** as a pale blue solid (0.487 g, 37%). X-ray quality crystals were grown by slow evaporation of a solution of sublimed **7** in hexane at 23 °C under an argon atmosphere: mp 73-76 °C, dec. 210 °C; IR (cm^{-1}) 2949 (m), 1616 (m), 1454 (m), 1330 (s), 1134 (s), 918 (m), 869 (m), 580 (m), 424 (m).

Anal. Calcd. for $C_{48}H_{96}Nd_2N_6O_6$: C, 50.49; H, 8.47; N, 7.36. Found: C, 49.99; H, 8.51; N, 7.14.

Preparation of $Lu(L^1)_3$ (8). In a fashion similar to the preparation of **7**, treatment of anhydrous $LuCl_3$ (0.655 g, 2.33 mmol) with a solution of KL^1 (prepared from L^1H (1.000 g, 6.98 mmol) and KH (0.336 g, 8.38 mmol) in tetrahydrofuran (30 mL)) was followed by stirring at ambient temperature for 20 h. Sublimation of the crude product at 95 °C/0.5 Torr afforded **8** (0.571 g, 40%) as white, X-ray quality crystals: mp 112-116 °C, dec. 255 °C; ^{1}H NMR (benzene-d_6, 23 °C, δ) 4.60 (s, 3 H, C***H***), 2.38 (s, 18 H, N(C***H***$_3$)$_3$), 1.24 (s, 27 H, C(C***H***$_3$)$_3$; ^{13}C{^{1}H} NMR (benzene-d_6, 23 °C, ppm) 167.61 (s, ***C***-O), 110.30 (s, ***C***HN), 48.75 (s, N(***C***H$_3$)$_2$), 35.65 (s, ***C***(CH$_3$)$_3$), 28.74 (s, C(***C***H$_3$)$_3$); IR (cm^{-1}) 2949 (m), 1618 (w), 1458 (m), 1334 (s), 1138 (s), 1010 (m), 921 (m), 867 (m), 592 (m).

Anal. Calcd. for $C_{24}H_{48}LuN_3O_3$: C, 47.92; H, 8.04; N, 6.98. Found: C, 48.06; H, 8.18; N, 6.91.

Preparation of $[La(L^2)_3]_2$ (9). In a fashion similar to the preparation of **7,** treatment of anhydrous $LaCl_3$ (0.483 g, 1.97 mmol) with a solution of KL^2 (prepared from L^2H (1.000 g, 5.92 mmol) and KH (0.284 g, 7.09 mmol) in tetrahydrofuran (30 mL)) afforded **9** (0.628 g, 50%) as white, X-ray quality crystals upon sublimation at 160 °C/0.5 Torr: mp 171 °C, dec. 180 °C; ^{1}H NMR (benzene-d_6, 23 °C, δ) 4.74 (s, 6 H, C***H***), 2.87 (br m, 24 H, N(C***H***$_2$)$_2$(CH$_2$)$_2$), 1.80 (br m, 24 H, N(CH$_2$)$_2$(C***H***$_2$)$_2$), 1.27 (s, 54 H, C(C***H***$_3$)$_3$); ^{13}C{^{1}H} NMR (benzene-d_6, 23 °C, ppm) 166.53 (s, ***C***-O), 105.64 (s, ***C***HN), 55.08 (s, N(***C***H$_2$)$_2$(CH$_2$)$_2$), 35.92 (s, ***C***(CH$_3$)$_3$), 28.99 (s, C(***C***H$_3$)$_3$), 24.04 (s, N(CH$_2$)$_2$(***C***H$_2$)$_2$); IR (cm^{-1}) 2956 (m), 1606 (m), 1477 (w), 1344 (m), 1325 (s), 1143 (s), 1097 (m), 920 (m), 572 (m), 475 (w).

Anal. Calcd. for $C_{60}H_{108}La_2N_6O_6$: C, 55.98; H, 8.46; N, 6.53. Found: C, 54.24; H, 8.37; N, 6.36.

Preparation of $La(L^3)_3$ (10). In a fashion similar to the preparation of **7**, treatment of anhydrous $LaCl_3$ (0.446 g, 1.82 mmol) with a solution of KL^3 (prepared from L^3H (1.000 g, 5.46 mmol) and KH (0.263 g, 6.55 mmol) in tetrahydrofuran (30 mL)) afforded **10** (0.490 g, 39%) as a white solid upon sublimation 155 °C/0.5 Torr: mp 140-144 °C, dec. 255 °C; ^{1}H NMR (benzene-d_6, 23 °C, δ) 4.79 (s, 3 H, C***H***), 2.84 (br m, 12 H, N(C***H***$_2$)$_2$(CH$_2$)$_2$(CH$_2$)), 1.76 (br m, 12 H, N(CH$_2$)$_2$(C***H***$_2$)$_2$(CH$_2$)), 1.36 (br m, 6 H, N(CH$_2$)$_2$(CH$_2$)$_2$(C***H***$_2$)), 1.29 (s, 27 H, C(C***H***$_3$)$_3$); ^{13}C{^{1}H} NMR (benzene-d_6, 23 °C, δ) 164.98 (s, ***C***-O), 105.36 (s, ***C***HN), 54.62 (s, N(***C***H$_2$)$_2$(CH$_2$)$_2$(CH$_2$)), 36.25 (s, ***C***(CH$_3$)$_3$), 29.25 (s, C(***C***H$_3$)$_3$), 24.78 (s, N(CH$_2$)$_2$(***C***H$_2$)$_2$(CH$_2$)), 24.28 (s, N(CH$_2$)$_2$(CH$_2$)$_2$(***C***H$_2$); IR (cm^{-1}) 2935 (s), 1576 (w), 1450 (w), 1335 (s), 1148 (m), 1093 (m), 1049 (m), 983 (m), 858 (m).

Anal. Calcd. for $C_{33}H_{60}LaN_3O_3$: C, 57.79; H, 8.82; N, 6.13. Found: C, 56.40; H, 8.94; N, 6.05.

Preparation of $Pr(L^3)_3$ (11). In a fashion similar to the preparation of **7**, treatment of anhydrous $PrCl_3$ (0.450 g, 1.82 mmol) with a solution of KL^3 (prepared from L^3H (1.000 g, 5.46 mmol) and KH (0.263 g, 6.55 mmol) in tetrahydrofuran (30 mL) afforded **11** (0.513 g, 41%) as a pale yellow-green solid upon sublimation at 150 °C/0.5 Torr: mp 124-128 °C, dec. 280 °C; IR (cm^{-1}) 2930 (m), 1618 (w), 1456 (w), 1454 (w), 1329 (m), 1145 (m), 1099 (m), 1091 (m), 725 (m), 581 (m).

Anal. Calcd. for $C_{33}H_{60}PrN_3O_3$: C, 57.63; H, 8.79; N, 6.11. Found: C, 52.42; H, 8.30; N, 5.60.

Preparation of $Nd(L^3)_3$ (12). In a fashion similar to the preparation of **7**, treatment of anhydrous $NdCl_3$ (0.456 g, 1.82 mmol) with a solution of KL^1 (prepared from L^3H (1.000 g, 5.46 mmol) and KH (0.263 g, 6.55 mmol) in tetrahydrofuran (30 mL)) afforded **12** (0.674, 54%) as a pale blue solid upon sublimation 160 °C/0.5 Torr: mp 144-148 °C, dec. 280 °C. IR (cm^{-1}) 2931 (s), 2852 (w), 1575 (w), 1454 (w), 1330 (s), 1147 (m), 1091 (m), 1053 (m), 981 (s), 860 (m), 570 (s).

Anal. Calcd. for $C_{33}H_{60}NdN_3O_3$: C, 57.35; H, 8.75; N, 6.08. Found: C, 55.84; H, 8.59; N, 6.03.

Preparation of $Er(L^3)_3$ (13). In a fashion similar to the preparation of **7**, treatment of anhydrous $ErCl_3$ (0.498 g, 1.82 mmol) with a solution of KL^3 (prepared from L^3H (1.000 g, 5.46 mmol) and KH (0.263 g, 6.55 mmol) in tetrahydrofuran (30 mL)) afforded **13** (0.613 g, 47%) as pink, X-ray quality crystals upon sublimation of the crude solid at 140 °C/0.5 Torr: mp 155-158 °C, dec. 290 °C; IR (cm^{-1}) 2931 (m), 1613 (m), 1450 (m), 1331 (s), 1146 (s), 1096 (m), 1043 (m), 987 (m), 923 (s), 696 (m), 586 (s).

Anal. Calcd. for $C_{33}H_{60}ErN_3O_3$: C, 55.50; H, 8.47; N, 5.88. Found: C, 54.33; H, 8.75; N, 5.81.

Preparation of $Lu(L^3)_3$ (14). In a fashion similar to the preparation of **7**, treatment of anhydrous $LuCl_3$ (0.512 g, 1.82 mmol) with a solution of KL^3 (prepared from L^3H (1.000 g, 5.46 mmol) and KH (0.263 g, 6.55 mmol) in tetrahydrofuran (30 mL)) afforded **14** (0.519 g, 40%) as a white solid upon sublimation at 140 °C/0.5 Torr: mp 167-172 °C, dec.

272 °C; ^{1}H NMR (benzene-d_6, 23 °C, δ) 4.96 (s, 3 H, C***H***), 2.92 (br m, 12 H, N(C***H***$_2$)$_2$(CH$_2$)$_2$(CH$_2$)), 1.71 (br m, 12 H, N(CH$_2$)$_2$(C***H***$_2$)$_2$(CH$_2$)), 1.38 (br m, 6 H, N(CH$_2$)$_2$(CH$_2$)$_2$(C***H***$_2$)), 1.27 (s, 27 H, C(C***H***$_3$)$_3$); ^{13}C{^{1}H} NMR (benzene-d_6, 23 °C, ppm) 167.05 (s, ***C***-O), 106.37 (s, ***C***HN), 56.52 (s, N(***C***H$_2$)$_2$(CH$_2$)$_2$(CH$_2$)), 35.83 (s, ***C***(CH$_3$)$_3$), 28.65 (s, C(***C***H$_3$)$_3$), 24.34 (s, N(CH$_2$)$_2$(***C***H$_2$)$_2$(CH$_2$)), 22.80 (s, N(CH$_2$)$_2$(CH$_2$)$_2$(***C***H$_2$)); IR (cm^{-1}) 2932 (m), 1616 (m), 1450 (m), 1384 (m), 1332 (s), 1145 (s), 1093 (m), 1043 (m), 987 (m), 923 (s), 860 (m), 590 (s).

Anal. Calcd. for $C_{33}H_{60}LuN_3O_3$: C, 54.91; H, 8.38; N, 5.82. Found: C, 52.09; H, 8.11; N, 5.61.

Preparation of Y(L^3)$_3$ (15). In a fashion similar to the preparation of **7**, treatment of anhydrous YCl_3 (0.355 g, 1.82 mmol) with a solution of KL^3 (prepared from L^{3}H (1.000 g, 5.46 mmol) and KH (0.263 g, 6.55 mmol) in tetrahydrofuran (30 mL)) afforded **15** (0.647 g, 56%) as a white solid upon sublimation at 160 °C/0.5 Torr: mp 152-155 °C, dec. 280 °C; ^{1}H NMR (benzene-d_6, 23 °C, δ) 4.88 (s, 3 H, C***H***), 2.91 (br m, 12 H, N(C***H***$_2$)$_2$(CH$_2$)$_2$(CH$_2$)), 1.71 (br m, 12 H, N(CH$_2$)$_2$(C***H***$_2$)$_2$(CH$_2$)), 1.38 (br m, 6 H, N(CH$_2$)$_2$(CH$_2$)$_2$(C***H***$_2$)), 1.27 (s, 27 H, C(C***H***$_3$)$_3$); ^{13}C{^{1}H} NMR (benzene-d_6, 23 °C, ppm) 166.48 (s, ***C***-O), 106.12 (s, ***C***HN), 55.92 (s, N(***C***H$_2$)$_2$(CH$_2$)$_2$(CH$_2$)), 35.64 (s, ***C***(CH$_3$)$_3$), 28.72 (s, C(***C***H$_3$)$_3$), 24.40 (N(CH$_2$)$_2$(***C***H$_2$)$_2$(CH$_2$)), 22.99 (s, N(CH$_2$)$_2$(CH$_2$)$_2$(***C***H$_2$)); IR (cm^{-1}) 2933 (m), 1612 (m), 1450 (m), 1381 (m), 1333 (s), 1146 (s), 1043 (m), 985 (m), 860 (m), 587 (s).

Anal. Calcd. for $C_{33}H_{60}YN_3O_3$: C, 62.34; H, 9.51; N, 6.61. Found: C, 60.42; H, 9.47; N, 6.46.

ASSOCIATED CONTENT

Supporting Information

X-ray diffraction data, NMR and infrared spectral data, and TGA analyses available as a PDF file (49 pages). The Supporting Information is available free of charge on the ACS Publications website.

Accession Codes

CCDC 2058137 (**1**), 2058125 (**2**), 2058126 (**3**), 2058129 (**7**), 2058127 (**8**), 2058130 (**9**), 2058128 (**13**), and 2058131 (**14**) contain the supplementary crystallographic data for this paper. These data can be obtained free of charge via www.ccdc.cam.ac.uk/data_request/cif, or by emailing data_request@ccdc.cam.ac.uk, or by contacting The Cambridge Crystallographic Data Centre, 12 Union Road, Cambridge CB2 1EZ, UK; fax: +44 1223 336033.

AUTHOR INFORMATION

Corresponding Author

*E-mail: chw@chem.wayne.edu

Notes

The authors declare no competing financial interest.

ACKNOWLEDGMENT

This research was primarily supported by the U.S. National Science Foundation through the University of Wisconsin Materials Research Science and Engineering Center (DMR-1720415). This work also made use of the powder X-ray diffraction facility at Wayne State University that was partially funded by U.S. National Science Foundation (grant no. CHE-1427926). The authors gratefully acknowledge the use of facilities and instrumentation at the UW-Madison Wisconsin Centers for Nanoscale Technology (wcnt.wisc.edu), which is partially supported by the U.S. National Science Foundation through the University of Wisconsin Materials Research Science and Engineering Center (DMR-1720415).

REFERENCES

(1) Wang, B.; Huang, W.; Chi, L.; Al-Hashimi, M.; Marks, T. J.; Facchetti, A. High-k Gate Dielectrics for Emerging Flexible and Stretchable Electronics. *Chem. Rev.* **2018**, *118*, 5690-5754.

(2) Robertson, J. High Dielectric Constant Oxides. *Eur. Phys. J. Appl. Phys.* **2004**, *28*, 265-291.

(3) Wiemer, C.; Lamagna, L.; Fanciulli, M. Atomic Layer Deposition of Rare-Earth-Based Binary and Ternary Oxides for Microelectronic Applications. *Semicond. Sci. Technol.* **2012**, *27*, 074013.

(4) Leskelä, M.; Kukli, K.; Ritala, M. Rare-Earth Oxide Thin Films for Gate Dielectrics in Microelectronics. *J. Alloys Compounds* **2006**, *418*, 27-34.

(5) Mikkulainen, V.; Leskelä, M.; Ritala, M.; Puurunen, R. L. Crystallinity of Inorganic Films Grown by Atomic Layer Deposition: Overview and General Trends. *J. Appl. Phys.* **2013**, *113*, 021301.

(6) Johnson, R. W.; Hulqvist, A.; Bent, S. F. A Brief Review of Atomic Layer Deposition: From Fundamentals to Applications. *Mater. Today* **2014**, *17*, 236-246.

(7) Lopes, J. M. J.; Özben, E. D.; Roeckerath, M.; Littmark, U.; Lupták, R.; Lenk, S.; Luysberg, M.; Besmehn, A.; Breuer, U.; Schubert, J.; Mantl, S. Amorphous Ternary Rare-Earth Gate Oxides for Future Integration in MOSFETs. *Microelectron. Eng.* **2009**, *86*, 1646-1649.

(8) Goh, K. H.; Haseeb, A. S. M. A.; Wong, Y. W. Lanthanide Rare Earth Oxide Thin Film as an Alternative Gate Oxide. *Mater. Sci. Semicond. Process*. **2017**, *68*, 302-315.

(9) de Rouffignac, P.; Gordon, R. G. Atomic Layer Deposition of Praseodymium Aluminum Oxide for Electrical Applications. *Chem. Vap. Deposition* **2006**, *12*, 152-157.

(10) Ohtomo, A.; Hwang, H. Y. A High Mobility Electron Gas at The $LaAlO_3$/$SrTiO_3$ Heterointerface. *Nature* **2004**, *427*, 423-426.

(11) Vasylechko, L.; Stepchuck, R.; Prots, Y.; Rosner, H. Concentration and Temperature Induced Phase Transitions in $PrAlO_3$-$SrTiO_3$ System. *Nanoscale Res. Lett.* **2016**, *11*, 17.

(12) Mannhart, J.; Blank, D. H. A.; Hwang, H. Y.; Millis, A. J.; Triscone, J. M. Two-Dimensional Electron Gases at Oxide Interfaces. *MRS Bull.* **2008**, *33*, 1027-1034.

(13) Reyren, N.; Thiel, S.; Caviglia, A. D.; Kourkoutis, L. F.; Hammerl, G.; Richter, C.; Schneider, C. W.; Kopp, T.; Ruetschi, A. S.; Jaccard, D.; Gabay, M.; Muller, D. A.; Triscone, J.-M.; Mannhart, J. Superconducting Interfaces Between Insulating Oxides. *Science* **2007,** *317*, 1196-1199.

(14) Brinkman, A.; Huijben, M.; van Zalk, M.; Huijben, J.; Zeitler, U.; Maan, J. C.; van der Wiel, W. G.; Rijnders, G.; Blank, D. H. A.; Hilgenkamp, H. Magnetic Effects at the Interface Between Non-Magnetic Oxides. *Nature Mater.* **2007,** *6*, 493-496.

(15) Thiel, S.; Hammerl, G.; Schmehl, A.; Schneider, C. W.; Mannhart, J. Tunable Quasi-Two-Dimensional Electron Gases in Oxide Heterostructures. *Science* **2006,** *313* (5795), 1942-1945.

(16) Ariando; Wang, X.; Baskaran, G.; Liu, Z. Q.; Huijben, J.; Yi, J. B.; Annadi, A.; Barman, A. R.; Rusydi, A.; Dhar, S.; Feng, Y.P.; Ding, J.; Hilgenkamp, H.; Venkatesan, T. Electronic Phase Separation at the $LaAlO_3$/$SrTiO_3$ Interface. *Nature Commun.* **2011,** *2*, 188.

(17) Bohr, M. T.; Chau, R. S.; Ghani, T.; Mistry, K. The High-k Solution. *IEEE Spectrum* **2007**, *44*, 29-35.

(18) Zhang, Q. Y.; Huang, X. Y. Recent Progress in Quantum Cutting Phosphors. *Progr. Mater. Sci.* **2010**, *55*, 353-427.

(19) Pénard, A.-L.; Gacoin, T.; Boilot, J.-P. Functionalized Sol-Gel Coatings for Optical Applications. *Acc. Chem. Res.* **2007**, *40*, 895-902.

(20) Liu, X.; Wen, F.; Karapetrova, E.; Kim, J.-W.; Ryan, P. J.; Freeland, J. W.; Terilli, M.; Wu, T.-C.; Kareev, M.; Chakhalian, J. In-Situ Fabrication and Transport Properties of (111) $Y_2Ir_2O_7$ Epitaxial Film. *Appl. Phys. Lett.* **2020**, *117*, 041903.

(21) Gaita-Arino, A.; Luis, F.; Hill, S.; Coronado, E. Molecular Spins for Quantum Computation. *Nature Chemistry* **2019**, *11*, 301-309.

(22) Jha, A. K.; Matsumoto, K. Superconductive REBCO Thin Films and Their Nanocomposites: The Role of Rare-Earth Oxides in Promoting Sustainable Energy. *Frontiers Phys.* **2019**, *7*, 82.

(23) Zeng, Z.; Xu, Y.; Zhang, Z.; Gao, Z.; Luo, M.; Yin, Z.; Zhang, C.; Xu, J.; Huang, B.; Luo, F.; Du, Y.; Yan, C. Rare-Earth-Containing Perovskite Nanomaterials: Design, Synthesis, Properties, and Applications. *Chem. Soc. Rev.* **2020**, *49*, 1109-1143.

(24) Biswas, A.; Yang, C.-H.; Ramesh, R.; Jeong, Y. H. Atomically Flat Single Terminated Oxide Substrate Surfaces. *Progr. Surf. Sci.* **2017**, *92*, 117-141.

(25) Catalano, S.; Gibert, M.; Fowlie, J.; Iniguez, J.; Triscone, J.-M.; Kreisel, Rare-Earth Nickelates $RNiO_3$: Thin Films and Heterostructures. *J. Rep. Prog. Phys.* **2018**, *81*, 046501.

(26) Leskelä, M.; Ritala, M. Atomic Layer Deposition Chemistry: Recent Developments and Future Challenges. *Angew. Chem. Int. Ed.* **2003**, *42*, 5548-5554.

(27) George, S. M. Atomic Layer Deposition: An Overview. *Chem. Rev.* **2010**, *110*, 111-131.

(28) Jang, J.; Moon, D.; Lee, H. J.; Lee, D.; Choi, D.; Bae, D.; Yuh, H.; Moon, Y.; Park, Y.; Yoon, E. Incorporation of Air-Cavity into Sapphire Substrate and its Effect on GaN Growth and Optical Properties. *J. Cryst. Growth* **2015**, *430*, 41-45.

(29) Devi, A. Old Chemistries' for New Applications: Perspectives for Development of Precursors for MOCVD and ALD Applications. *Coord. Chem. Rev.* **2013**, *257*, 3332-3384.

(30) Tiitta, M.; Niinistö, L. Volatile Metal β-Diketonates: ALD and CVD Precursors for Electroluminescent Device Thin Films. *Chem. Vap. Deposition* **1997**, *3*, 167-182.

(31) Sønsteby, H. H.; Østreng, E.; Fjellvåg, H.; Nilsen, O. Deposition and X-Ray Characterization of Epitaxial Thin Films of $LaAlO_3$. *Thin Solid Films* **2014**, *50*, 90-94.

(32) Hansen, P.-A.; Fjellvåg, H.; Finstad, T.; Nilsen, O. Structural and Optical Properties of Lanthanide Oxides Grown by Atomic Layer Deposition (Ln = Pr, Nd, Sm, Eu, Tb, Dy, Ho, Er, Tm, Yb). *Dalton Trans.* **2013**, *42*, 10778-10785.

(33) Zhao, L.; Liu, H.-X.; Wang, X.; Fei, C.-X.; Feng, X.-Y.; Wang, Y.-T. Effects of Annealing Ambient on the Characteristics of $LaAlO_3$ Films Grown by Atomic Layer Deposition. *Nanoscale Res. Lett.* **2017**, *12*, 108.

(34) Oh, I.-K.; Kim, K.; Lee, Z.; Ko, K. Y.; Lee, C.-W.; Lee, S. J.; Myung, J. M.; Lansalot-Matras, C.; Noh, W.; Dussarrat, C.; Kim, H.; Lee, H.-B.-R. Hydrophobicity of Rare Earth Oxides Grown by Atomic Layer Deposition. *Chem. Mater.* **2015**, *27*, 148-156.

(35) Waduge, W. L. I.; Chen, Y.; Zuo, P.; Jayakodiarachchi, N.; Kuech, T. F.; Babcock, S. E.; Evans, P. G.; Winter, C. H. Solid-Phase Epitaxy of Perovskite High Dielectric $PrAlO_3$ Films Grown by Atomic Layer Deposition for Use in Two-Dimensional Electronics and Memory Devices. *ACS Appl. Nano Mater.* **2019**, *2*, 7449-7458.

(36) Blanquart, T.; Kaipio, M.; Niinistö, J.; Gavagnin, M.; Longo, V.; Blanquart, L.; Lansalot, C.; Noh, W.; Wanzenböck, H. D.; Ritala, M.; Leskelä, M. Cyclopentadienyl Precursors for the Atomic Layer Deposition of Erbium Oxide Thin Films. *Chem. Vap. Deposition* **2014**, *20*, 217-223.

(37) Jones, A. C.; Aspinall, H. C.; Chalker, P. R.; Potter, R. J.; Manning, T. D.; Loo, Y. F.; O'Kane, R.; Gaskell, J. M.; Smith, L. M. MOCVD and ALD of High-k Dielectric Oxides Using Alkoxide Precursors. *Chem. Vap. Deposition* **2006**, *12*, 83-98.

(38) Ngo, T. Q.; Posadas, A.; McDaniel, M. D.; Ferrer, D. A.; Bruley, J.; Breslin, C.; Demkov, A. A.; Ekerdt, J. G. Epitaxial Growth of $LaAlO_3$ on $SrTiO_3$-Buffered Si(001) Substrates by Atomic Layer Deposition. *J. Cryst. Growth* **2013**, *363*, 150-157.

(39) Seppälä, S.; Niinistö, J.; Blanquart, T.; Kaipio, M.; Mizohata, K.; Räisänen, J.; Lansalot-Matras, C.; Noh, W.; Ritala, M.; Leskelä, M. Heteroleptic Cyclopentadienyl-Amidinate Precursors for Atomic Layer Deposition (ALD) of Y, Pr, Gd, and Dy Oxide Thin Films. *Chem. Mater.* **2016**, *28*, 5440-5449.

(40) Xu, K.; Chaudhuri, A. R.; Parala, H.; Schwendt, D.; de lost Arcos, T.; Osten, H. J.; Devi, A. Atomic Layer Deposition of Er_2O_3 Thin Films from Er Tris-guanidinate and Water: Process Optimization, Film Analysis, and Electrical Properties. *J. Mater. Chem. C* **2013**, *1*, 3939-3946.

(41) Edelmann, F. T. Lanthanide Amidinates and Guanidinates in Catalysis and Materials Science: A Continuing Success Story. *Chem. Soc. Rev.* **2012**, *41*, 7657-7672.

(42) Mai, L.; Boysen, N.; Subasi, E.; de los Arcos, T.; Rogalla, D.; Grundmeier, G.; Bock, C.; Lu, H.-L.; Devi, A. Water Assisted Atomic Layer Deposition of Yttrium Oxide Using Tris(N,N'-diisopropyl-2-diemthylamido-guanidinato)yttrium(III): Process Development, Film Characterization, and Functional Properties. *RSC Advances* **2018**, *8*, 4987-4994.

(43) Kurek, A.; Gordon, P. G.; Karle, S.; Devi, A.; Barry, S. T. Recent Advances Using Guanidinate Ligands for Chemical Vapor Deposition (CVD) and Atomic Layer Deposition (ALD) Applications. *Aust. J. Chem.* **2014**, *67*, 989-996.

(44) Daly, S. R.; Kim, D. Y.; Girolami, G. S. Lanthanide N,N-Dimethylaminodiboranates as a New Class of Highly Volatile Chemical Vapor Deposition Precursors. *Inorg. Chem.* **2012**, *51*, 7050-7065.

(45) Vlaisavljevich, B.; Miro, P.; Koballa, D.; Todorova, T. K.; Daly, S. R.; Girolami, G. S.; Cramer, C. J.; Gagliardi, L. Volatilities of Actinide and Lanthanide N,N-Dimethylaminodiboranate Chemical Vapor Deposition Precursors: A DFT Study. *J. Phys. Chem. C* **2012**, *116*, 23194-23200.

(46) Daly, S. R.; Kim, D. Y.; Yang, Y.; Abelson, J. R.; Girolami, G. S. Lanthanide N,N-Dimethylaminodiboranates: Highly Volatile Precursors for the Deposition of Lanthanide-Containing Thin Films. *J. Am. Chem. Soc.* **2010**, *132*, 2106.

(47) Bordwell, F. G.; Harrelson, J. A. Jr.; Lynch, T.-Y. Homolytic Bond Dissociation Energies for the Cleavage of α-N-H Bonds in Carboxamides, Sulfonamides, and Their Derivatives. The Question of Synergism in Nitrogen-Centered Radicals. *J. Org. Chem.* **1990**, *55*, 3337-3341.

(48) Silverstein, T. P.; Heller, S. T. pKa Values in the Undergraduate Curriculum: What is the Real pKa of Water? *J. Chem. Educ.* **2017**, *94*, 690-695.

(49) Cozzi, P. G.; Veya, P.; Floriani, C.; Chiesi-Villa, A.; Rizzoli, C. β-Keto Amino Enolates Binding to Transition Metals: Synthesis and Structure of the Ion-Pair Form and Its Mono- and Bidentate Coordination to Zirconium and Nickel. *Organometallics* **1994**, *13*, 1528-1532.

(50) Van Vliet, M. R. P.; Jastrzebski, J. T. B. H.; Van Koten, G.; Vrieze, K.; Spek, A. L. Novel Reactions of Substituted 1-Aza-4-oxobutadienes (α-Iminoketones) with Diorganozinc Reagents. Selective Ethyl Transfer in the Et_2Zn/t-BuN=C(H)-C(Me)=O System and X-Ray Crystal Structure of $[EtZn(Et)(t\text{-}Bu)NC(H)=C(Me)O]_2$. *J. Organomet. Chem.* **1983**, *251*, C17-C21.

(51) Van Vliet, M. R. P.; Van Koten, G.; Buysingh, P.; Jastrzebski, J. T. B. H.; Spek, A. L. Reactivity of 1-Aza-4-oxa-1,3-butadienes (α-Imino Ketones) Toward Diorganozinc Reagents: Regio- and Chemoselective Transfer of Organo Groups in the $Et_2Zn/R^1N=C(R^2)\text{-}C(R^3)=O$ System and X-Ray Crystal Structure of the Organozinc Enolate $[EtZn(Et)(t\text{-}Bu)NC(H)=C(Me)O]_2$. *Organometallics* **1987**, *6*, 537-546.

(52) Pipko, S. E.; Balitzky, Y. V.; Sinitsa, A. D.; Gololobov, Y. G. Peculiarities of Structure and Properties of Phosphorus-Containing Cations with Two Intramolecular Donor-Acceptor Bonds N→P. Synthesis of the First 5-Coordinated P-Cation with P=N Bond. *Tetrahedron Lett.* **1994**, *35*, 165-168.

(53) Kilimann, U.; Schäfer, M.; Herbst-Immer, R.; Edelmann, F. T. Cyclooctatetraenyl-Komplexe der Frühen Ubergangsmetalle und Lanthanoide. III. Cyclooctatetraenyl-Lanthanoidtriflate und -Iodide: Neue Ausgangsmaterialien für die Organolanthanoid-Chemie. *J. Organomet. Chem.* **1994***, 469*, C10-C14.

(54) Hatanpää, T.; Kukli, K.; Mikko Ritala, M. Leskelä, M. Crystal Structures and Thermal Properties of Some Rare Earth Alkoxides with Tertiary Alcohols: Possible Precursors for Atomic Layer Deposition of Rare Earth Oxides. *J. Therm. Anal. Calorim*. **2011,** *105,* 61-71.

(55) Anwander, R.; Munck, F. C.; Priermeier, T.; Scherer, W.; Runte, O.; Herrmann, W. A. Volatile Donor-Functionalized Alkoxy Derivatives of Lutetium and Their Structural Characterization. *Inorg. Chem.* **1997**, *36*, 3545-3552.

(56) Aspinall, H. C.; Bickley, J. F.; Gaskell, J. M.; Jones, A. C.; Labat, G.; Chalker, P. R.; Williams, P. A. Precursors for MOCVD and ALD of Rare Earth Oxides-Complexes of the Early Lanthanides with a Donor-Functionalized Alkoxide Ligand. *Inorg. Chem.* **2007**, *46*, 15, 5852-5860.

(57) Aspinall, H. C.; Bacsa, J.; Jones, A. C.; Wrench, J. S.; Black, K.; Chalker, P. R.; King, P. J.; Marshall, P.; Werner, M.; Davies, H. O.; Odedra, R. Ce(IV) Complexes with Donor-Functionalized Alkoxide Ligands: Improved Precursors for Chemical Vapor Deposition of CeO_2. *Inorg. Chem.* **2011**, *50*, 11644-11652.

(58) Greenwood, N. N.; Earnshaw, A. *Chemistry of the Elements*; Pergamon Press: Oxford, U.K.; 2nd Ed.; 1997, pp. 946, 1223.

(59) Li, Z.; Xue, M.; Yao, H.; Sun, H.; Zhang, Y.; Shen, Q. Enol-Functionalized N-Heterocyclic Carbene Lanthanide Amide Complexes: Synthesis, Molecular Structures and Catalytic Activity for Addition of Amines to Carbodiimides. *J. Organomet. Chem.* **2012**, *713*, 27-34.

(60) Liu, R.; Zheng, P.; Weng, L.; Zhou, X.; Liu, C. Insertion of Ketenes into Lanthanocene n-Butylamide and Imidazolate Complexes. *J. Organomet. Chem.* **2008**, *693*, 1614-1620.

(61) Zhang, C.; Lin, Y.; Chen, Z.; Zhou, X. Insertion Reactions of PhEtCCO and PhNCO into Ln-S (Ln = Er, Y, Tb) Bond of $[Cp_2Ln(\mu\text{-}SEt)]_2$. *J. Rare Earths* **2006**, *24*, 9-14.

(62) Zhang, C.; Liu, R.; Zhou, X.; Chen, Z.; Weng, L.; Lin, Y. Insertion Reaction of Ketene into the Metal-Sulfur Bond: Synthesis and Characterization of $[Cp_2Ln(\mu\text{-}\eta^1\text{:}\eta^2\text{-}OC(SEt)=CPh_2]_2$ (Ln = Yb, Er, Sm, Y) and $[Cp_2Er(\mu\text{-}\eta^1\text{:}\eta^2\text{-}OC(SEt)=CPhEt]_2$. *Organometallics* **2004**, *23*, 3246-3521.

(63) Deacon, G. B.; Junk, P. C.; Moxey, G. J. Mono-, Di-, Tri- and Tetranuclear Rare Earth Complexes Obtained Using a Moderately Bulky Arloxide Ligand. *Chem. Asian J.* **2009**, *4*, 1717-1728.

(64) Barnhart, D. M.; Clark, D. L.; Gordon, J. C.; Huffman, J. C.; Vincent, R. L.; Watkin, J. G.; Zwick, B. D. Synthesis, Properties, and X-Ray Structures of the Lanthanide h6-Arene-Bridged Alkoxide Dimers $Ln_2(O\text{-}2,6\text{-}i\text{-}Pr_2C_6H_3)_6$ and Their Lewis Base Adducts $Ln(O\text{-}2,6\text{-}i\text{-}Pr_2C_6H_3)_3(THF)_2$ (Ln = Pr, Nd, Sm, Gd, Er, Yb, Lu). *Inorg. Chem.* **1994**, *33*, 3487-3497.

(65) Christidis, P. C.; Tossidis, I. A.; Paschalidis, D. G.; Tzavellas, L. C. Tris(acetylacetonato)(1,10-phenathroline)cerium(III) and Tris(acetylacetonato)(1,10-phenathroline)praseodymium(III). *Acta Crystallograph. Sect. C* **1998**, *C54*, 1233-1236.

(66) Feng, J.; Yu, J.-B.; Song, S.-Y.; Sun, L.-N.; Fan, W.-Q.; Guo, X.-M.; Dang, S.; Zhang, H.-J. Near-Infrared Luminescent Xerogel Materials Covalently Bonded with Ternary Lanthanide [Er(III), Nd(III), Yb(III), Sm(III)] Complexes. *Dalton Trans.* **2009**, 2406-2414.

(67) Bi, Y.; Guo, Y.-N.; Zhao, L.; Guo, Y.; Lin, S.-Y.; Jiang, S.-D.; Tang, J.; Wang, B.-W.; Gao, S. Capping Ligand Perturbed Slow Magnetic Relaxation in Dysprosium Single-Ion Magnets. *Chem. Eur. J.* **2011**, *17*, 12476-12481.

(68) Rogachev, A. Y.; Mironov, A. V.; Troyanov, S. I.; Kuzmina, N. P.; Nemukhin, A. V. Synthesis, Crystal Structures and Theoretical Study of Mixed Ligand Complexes of Lanthanides Acetylacetonates with o-Phenanthroline and 2,2′-dipyridyl: The Unexpected Inverted Electrostatic Trend in Stability. *J. Mol. Struct.* **2006**, *789*, 187-194.

(69) Wiedmann, M. K.; Karunarathne, M. C.; Baird, R. J.; Winter, C. H. Growth of Tantalum(V) Oxide Films by Atomic Layer Deposition Using the Highly Thermally Stable Precursor $Ta(NtBu)(iPrNC(Me)NiPr)_2(NMe_2)$. *Chem. Mater.* **2010**, *22*, 4400-4405.

(70) Dezelah, C. L. IV; El-Kadri, O. M.; Kukli, K.; Arstila, K.; Baird, R. J.; Lu, J.; Niinistö, L.; Winter, C. H. A Low Valent Metalorganic Precursor for the Growth of Tungsten Nitride Thin Films by Atomic Layer Deposition. *J. Mater. Chem.* **2007**, *17*, 1109-1116.

(71) Päiväsaari J.; Niinistö, J.; Arstila, K.; Kukli, K.; Putkonen, M.; Niinistö, L. High Growth Rate of Erbium Oxide Thin Films in Atomic Layer Deposition from $(CpMe)_3Er$ and Water Precursors. *Chem. Vap. Deposition* **2005**, *11*, 415-419.

(72) Streiwieser, A. Jr.; Nebenzahl, L. L. Carbon Acidity. LII. Equilibrium Acidity of Cyclopentadiene in Water and in Cyclohexylamine. *J. Am. Chem. Soc.* **1976**, *98*, 2188-2190.

(73) de Rouffignac, P.; Gordon, R. G. Atomic Layer Deposition of Praseodymium Aluminum Oxide for Electrical Applications. *Chem. Vap. Deposition* **2006**, *12*, 152-157.

(74) Sbrockey, N. M.; Luong, M.; Gallo, E. M.; Sloppy, J. D.; Chen, G.; Winkler, C. R.; Johnson, S. H.; Taheri, M. L.; Tompa, G. S.; Spanier, J. E. $LaAlO_3/SrTiO_3$ Epitaxial Heterostructures by Atomic Layer Deposition. *J. Electron. Mater.* **2012**, *41*, 819-823.

(75) Rao, V. P.; Besancon, B.; Omarjee, V.; Dussarrat, C. Development of Lanthanide Precursors as Dopants for Advanced High-k Materials. *ECS Trans.* **2010**, *33*, 145-156.

(76) Frenzel, T.; Beale, J. M.; Kobayashi, M.; Zenk, M. H.; Floss, H. G. Stereochemistry of Enzymatic Formation of the Berberine Bridge in Protoberberine Alkaloids. *J. Am. Chem. Soc*. **1988**, *110*, 7878-7880.

(77) Hoard, D. W.; Moher, E. D.; Turpin, J. A. Synthesis of *(R)*-(-)-1-Piperidino-3,3-dimethylbutan-2-ol: Application in the Molar Scale Asymmetric Ethylation of *trans*-Crotonaldehyde. *Org. Proc. Res. Dev.* **1999**, *3*, 64-66.

(78) Arachchilage, H. J.; Suescun, L.; Ward, C. L.; Winter, C. H. Volatile and Thermally Stable Silver Pyrazolate Complexes Containing N-Heterocyclic Carbene Ligands. *Polyhedron* **2021**, *197*, 115010.

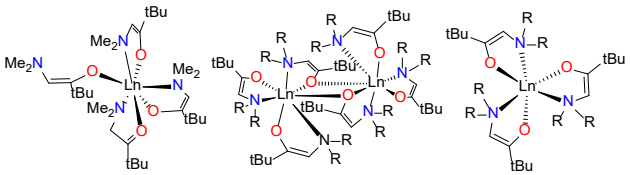
Ln = La, Pr, Nd, Er, Lu, Y